Space-Filling Curves and Applications in Electronic and Information Engineering

Maciej Ogorzałek
Department od Information Technologies
Faculty of Physics, Astronomy
and Applied Computer Science
Jagiellonian University
Kraków, Poland

Contents

Curve definition

If $\vec{f}:[a,b]\subset\mathbb{R}\longrightarrow\mathbb{R}^n$ is continuous, then $\vec{f}([a,b])$ is called a curve. Without loss of generality we can assume the domain to be *I*, *f*(0) and *f*(1) are the beginning and endpoint.

Notation: $f(t)=x=(x_1,x_2(,x_3)),t\in I$

Parameter representation with component functions:

$$\begin{cases} x_1=\varphi(t) \\ x_2=\psi(t) \\ (x_3=\chi(t)) \end{cases}$$

Space-filling curve (SFC) definition

Curves that pass through every point of an *n*-dimensional region with positive area (for *n*=2) or volume (for *n*=3), such as the unit square Ω in R^2 or the unit cube in R^3, are called space-filling curves.

Two main characteristics:

- continuous
- surjective

It can be shown that if *f* generates a space-filling curve, then it can not be bijective.

Contents

The Hilbert curve: geometric generation

- If *I* can be mapped continuously on Ω, then after partitioning *I* into four congruent subintervals and Ω into four congruent subsquares, each subinterval can be mapped continuously onto one of the subsquares. This partitioning can be carried out ad infinitum.
- The subsquares must be arranged such that adjacent subintervals are mapped onto adjacent subsquares.
- Inclusion relationship: if an interval corresponds to a square, then its subintervals must correspond to the subsquares of that square.
- This process defines a mapping $f_h(I)$, called the Hilbert space-filling curve.

The Hilbert curve: geometric generation

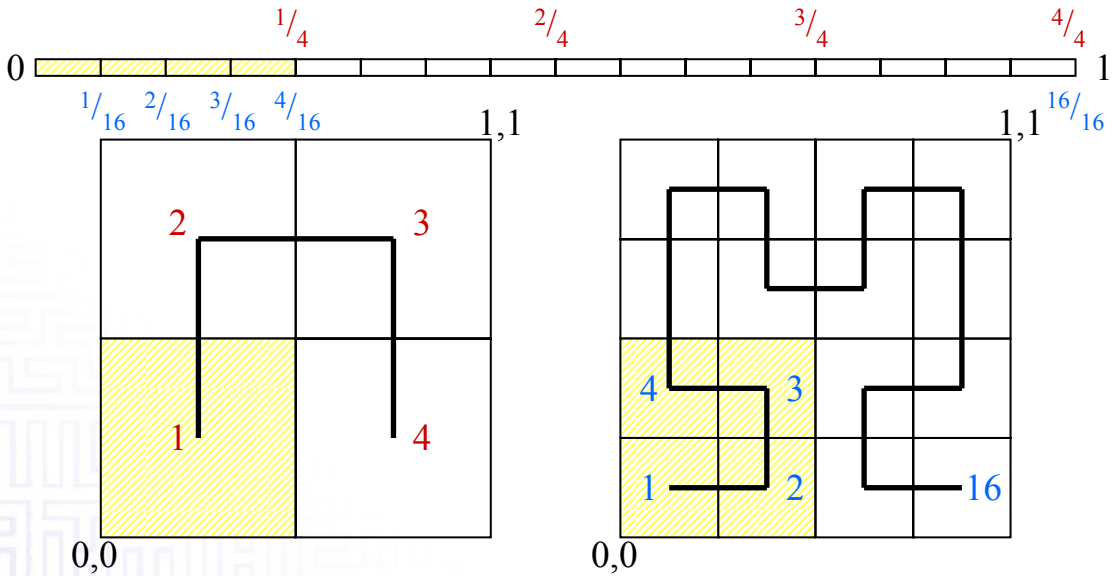

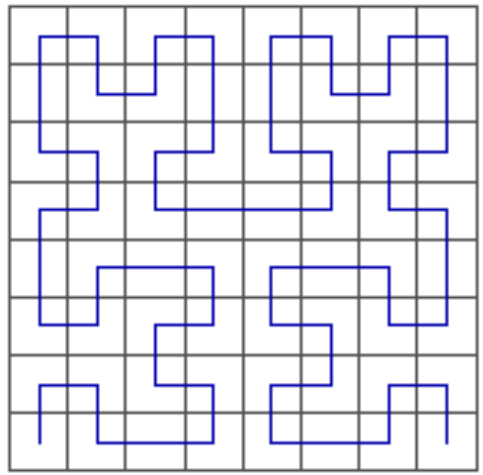

1st iteration

2nd iteration

3rd iteration

The Hilbert curve: geometric generation

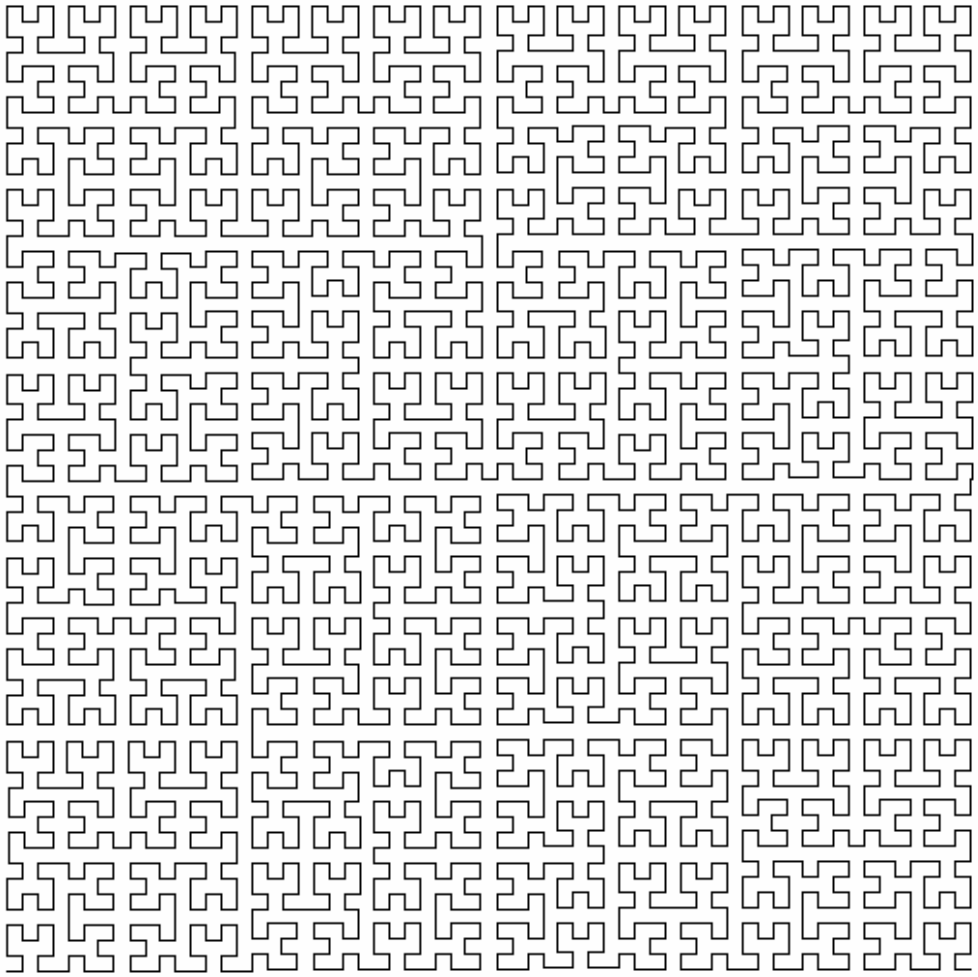

6th iteration

The Hilbert curve: geometric generation

The mapping $f_h : I \longrightarrow \Omega$ is surjective: with every sequence of nested closed squares corresponds a sequence of nested closed intervals that define a unique $t_0 \in I$.

The mapping $f_h : I \xrightarrow{onto} \Omega$ is continuous: in the *n*-th iteration *I* is partitioned in 2^{2n} subintervals, thus

$$t_1, t_2 \in I \ni \left|t_1 - t_2\right| < 1/2^{2n} \ then \left\| f_h(t_1) - f_h(t_2) \right\| \leq \sqrt{5}/2^n$$

The mapping $f_h : I \xrightarrow{onto} \Omega$ is nowhere differentiable.

The Hilbert curve: a complex representation [Sagan]

- Establish a formula to calculate the exact coordinates of an image point if

$$t = k / 2^{2n},\ n = 0,1,2,3,...,\ k = 0,1,2,3,...2^{2n}$$

- Use complex representation $z \in Z$, and affine transformations to wich Ω will be subjected recursively.
- Give an orientation to each subsquare such that the exit point of a subsquare coincides with the entry point of the next subsquare.

The Hilbert curve: a complex representation

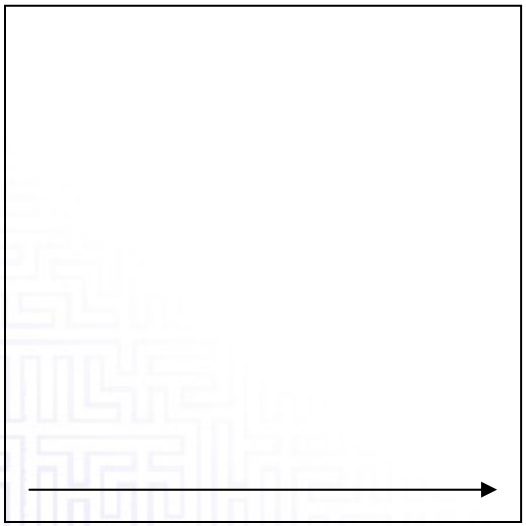

0th iteration

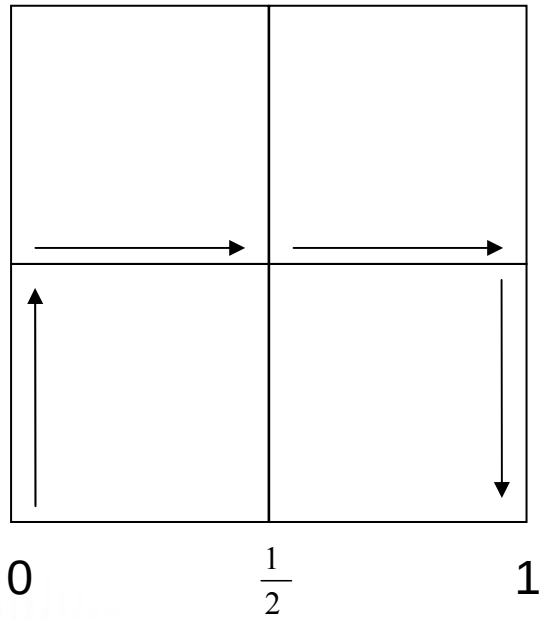

1st iteration

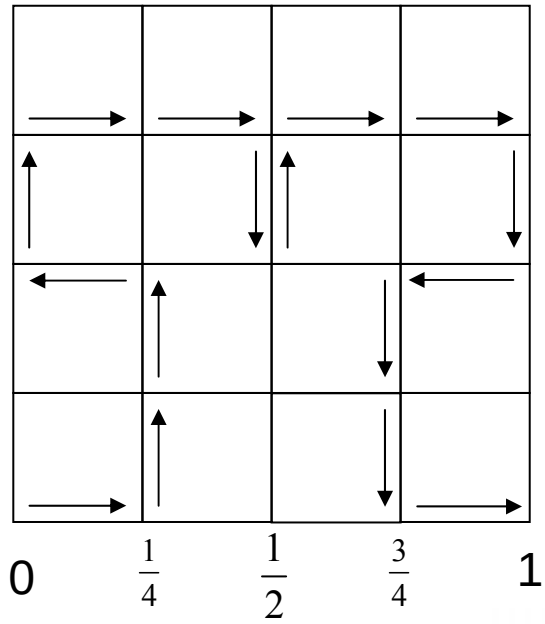

2nd iteration

The Hilbert curve: a complex representation

The four basic transformations (2 dimensional case):

$$\boldsymbol{h}_0 z = \frac{1}{2}\bar{z}i \qquad : \boldsymbol{h}_0 \begin{pmatrix} x_1 \\ x_2 \end{pmatrix} = \frac{1}{2}\begin{bmatrix} 0 & 1 \\ 1 & 0 \end{bmatrix}\begin{pmatrix} x_1 \\ x_2 \end{pmatrix} + \frac{1}{2}\begin{pmatrix} 0 \\ 0 \end{pmatrix} = \frac{1}{2}H_0\begin{pmatrix} x_1 \\ x_2 \end{pmatrix} + \frac{1}{2}h_0$$

$$\boldsymbol{h}_1 z = \frac{1}{2}z + \frac{i}{2} \qquad : \boldsymbol{h}_1 \begin{pmatrix} x_1 \\ x_2 \end{pmatrix} = \frac{1}{2}\begin{bmatrix} 1 & 0 \\ 0 & 1 \end{bmatrix}\begin{pmatrix} x_1 \\ x_2 \end{pmatrix} + \frac{1}{2}\begin{pmatrix} 0 \\ 1 \end{pmatrix} = \frac{1}{2}H_1\begin{pmatrix} x_1 \\ x_2 \end{pmatrix} + \frac{1}{2}h_1$$

$$\boldsymbol{h}_2 z = \frac{1}{2}z + \frac{1}{2} + \frac{i}{2} \qquad : \boldsymbol{h}_2 \begin{pmatrix} x_1 \\ x_2 \end{pmatrix} = \frac{1}{2}\begin{bmatrix} 1 & 0 \\ 0 & 1 \end{bmatrix}\begin{pmatrix} x_1 \\ x_2 \end{pmatrix} + \frac{1}{2}\begin{pmatrix} 1 \\ 1 \end{pmatrix} = \frac{1}{2}H_2\begin{pmatrix} x_1 \\ x_2 \end{pmatrix} + \frac{1}{2}h_2$$

$$\boldsymbol{h}_3 z = -\frac{1}{2}\bar{z}i + 1 + \frac{i}{2} \qquad : \boldsymbol{h}_3 \begin{pmatrix} x_1 \\ x_2 \end{pmatrix} = \frac{1}{2}\begin{bmatrix} 0 & -1 \\ -1 & 0 \end{bmatrix}\begin{pmatrix} x_1 \\ x_2 \end{pmatrix} + \frac{1}{2}\begin{pmatrix} 2 \\ 1 \end{pmatrix} = \frac{1}{2}H_3\begin{pmatrix} x_1 \\ x_2 \end{pmatrix} + \frac{1}{2}h_3$$

The Hilbert curve: a complex representation

- Represent $t \in I$ as $t = 0_4 q_1 q_2 q_3 ..., \; with \; q_j = 0,1,2 \; or \; 3$
- $f_h(t) \in \boldsymbol{h}_{q_1} \Omega$, $f_h(t) \in \boldsymbol{h}_{q_1} \boldsymbol{h}_{q_2} \Omega$, ad infinitum:

$$f_h(t) = \lim_{n \to \infty} \boldsymbol{h}_{q_1} \boldsymbol{h}_{q_2} \boldsymbol{h}_{q_3} ... \boldsymbol{h}_{q_n} \Omega$$

- For finite quaternaries (edges of subintervals in *n*th iteration):

$$f_h(0_4 q_1 q_2 q_3 ... q_n) = \boldsymbol{h}_{q_1} \boldsymbol{h}_{q_2} \boldsymbol{h}_{q_3} ... \boldsymbol{h}_{q_n} \underbrace{\boldsymbol{h}_0 \boldsymbol{h}_0 \boldsymbol{h}_0 ...}_{} \Omega$$

$$f_h(0_4 q_1 q_2 q_3 ... q_n) = \boldsymbol{h}_{q_1} \boldsymbol{h}_{q_2} \boldsymbol{h}_{q_3} ... \boldsymbol{h}_{q_n} \begin{pmatrix} 0 \\ 0 \end{pmatrix}$$

The Hilbert curve: a complex representation

- continued...

$$\boldsymbol{h}_{q_1}\boldsymbol{h}_{q_2}\boldsymbol{h}_{q_3}\ldots\boldsymbol{h}_{q_n}\begin{pmatrix}0\\0\end{pmatrix}=\ldots=\sum_{j=1}^{n}\left(\frac{1}{2^j}\right)H_{q_0}H_{q_1}H_{q_2}H_{q_3}\ldots H_{q_{j-1}}h_{q_j}$$

$$f_h \text{ is cont.} \Rightarrow \quad f_h(0_4 q_1 q_2 q_3\ldots)=\sum_{j=1}^{\infty}\left(\frac{1}{2^j}\right)H_{q_0}H_{q_1}H_{q_2}H_{q_3}\ldots H_{q_{j-1}}h_{q_j}$$

- Taking into account some properties of H_{q_j} :

$$f_h(0_4 q_1 q_2 q_3\ldots)=\sum_{j=1}^{\infty}\left(\frac{1}{2^j}\right)H_0^{e_{0j}}H_3^{e_{3j}}h_{q_j}\ ,$$

with e_{kj} = *number of* k*'s preceding* $q_j \pmod 2$, $k=0$ *or* 3

The Hilbert curve: a complex representation

- Further simplifications of the formula are possible...
- An example: $f_h(0_4203) = \boldsymbol{h}_2\boldsymbol{h}_0\boldsymbol{h}_3 \begin{pmatrix} 0 \\ 0 \end{pmatrix} = \begin{pmatrix} 5/8 \\ 3/4 \end{pmatrix}$

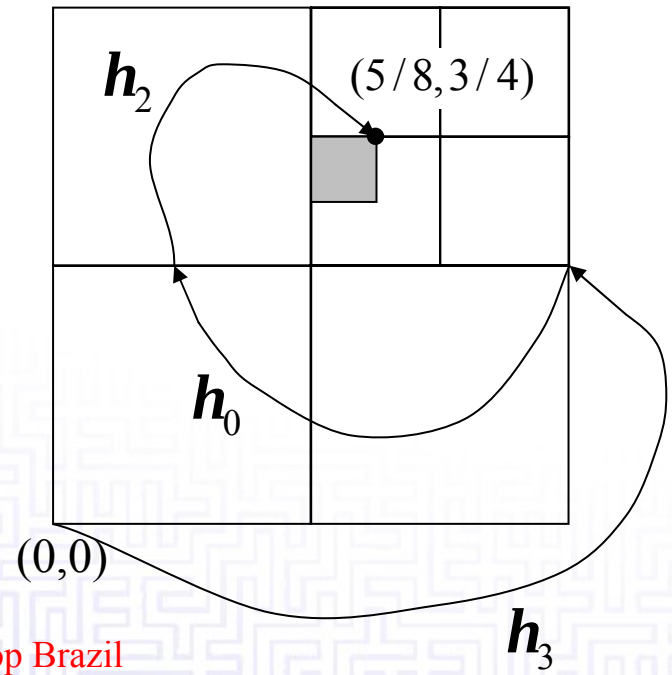

Approximating polygons for the Hilbert curve

The polygonal line that runs through the points

$$f_h(0), f_h(1/2^{2n}), f_h(2/2^{2n}), f_h(3/2^{2n}),..., f_h((2^{2n}-1)/2^{2n}), f_h(1),$$

is called the *n*th approximating polygon or a discrete space filling curve.

Parametrization:

$$p_n : I \to \Omega : p_n(t) = 2^{2n}(t - \frac{k}{2^{2n}}) f_h(\frac{k+1}{2^{2n}}) - 2^{2n}(t - \frac{k+1}{2^{2n}}) f_h(\frac{k}{2^{2n}}),$$

$$for\ k/2^{2n} \le t \le (k+1)/2^{2n}, k = 0,1,2,3,...2^{2n}-1$$

$\{p_n\}$ converges uniformly to the Hilbert curve

The Hilbert curve: representation through grammars

- Make use of four distinct templates to generate the discrete Hilbert curve: *H,A,B* and *C.*
- These templates will be translated to a first iteration of the curve according to a fixed scheme.

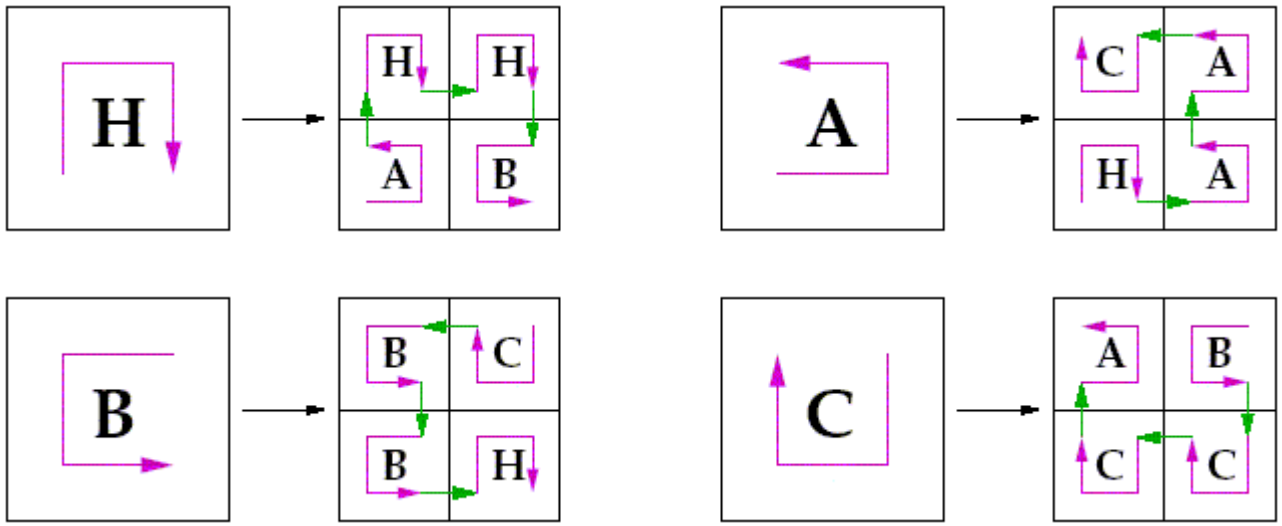

The Hilbert curve: representation through grammars

$$
\begin{aligned}
H &\longleftarrow A \uparrow H \rightarrow H \downarrow B \\
A &\longleftarrow H \rightarrow A \uparrow A \leftarrow C \\
B &\longleftarrow C \leftarrow B \downarrow B \rightarrow H \\
C &\longleftarrow B \downarrow C \leftarrow C \uparrow A
\end{aligned}
$$

- The resulting rules and transitions can be used to implement the recursive construction of the discrete Hilbert curve.

$$
\begin{aligned}
H &\longleftarrow A \uparrow H \rightarrow H \downarrow B \\
&\longleftarrow H \rightarrow A \uparrow A \leftarrow C \uparrow A \uparrow H \rightarrow H \downarrow B \rightarrow A \uparrow H \rightarrow H \downarrow B \downarrow C \leftarrow B \downarrow B \rightarrow H
\end{aligned}
$$

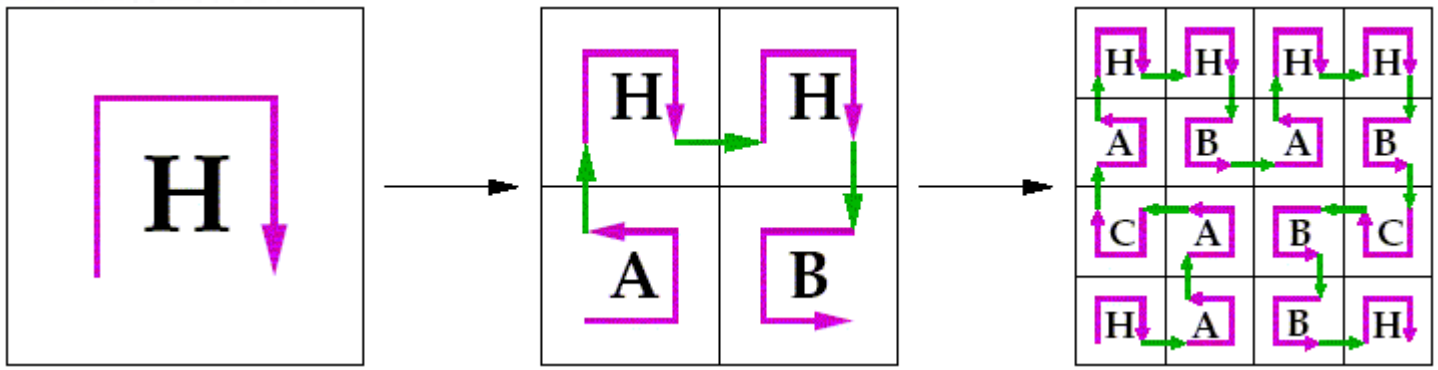

Contents

1. Introductory section
2. Types of space-filling curves
    1. The Hilbert space-filling curve
    2. The Peano space-filling curve
    3. The Sierpinski space-filling curve
    4. The Lebesgue space-filling curve
3. Application of space-filling curves

The Peano curve: definition

- $f_p : I \to \Omega$ with

$$f_p(0_3 t_1 t_2 t_3 t_4 \ldots) = \begin{pmatrix} 0_3 t_1 (k^{t_2} t_3)(k^{t_2+t_4} t_5)\ldots \\ 0_3 (k^{t_1} t_2)(k^{t_1+t_3} t_4)\ldots \end{pmatrix}$$

$$with \;\; kt_j = 2 - t_j \;\; (t_j = 0,1,2) \;\; and \;\; k^{\nu} \; is \; the \; \nu th \; it. \; of \; k$$

is surjective and continuous on *I*, and represents a SFC.

- More interesting: geometric generation according to Hilbert

The Peano curve: a complex representation

- Define orientation of the subsquares:

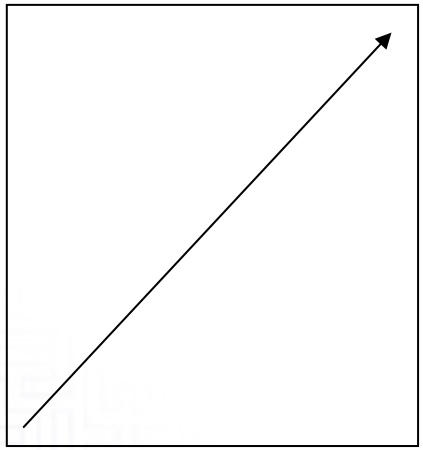

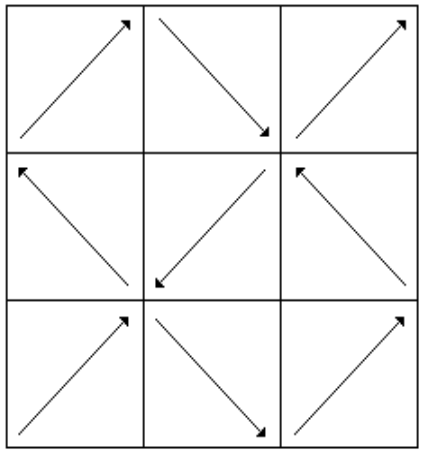

- Define similarity transforms: $\boldsymbol{p}_0 z = \frac{1}{3} z,\ \boldsymbol{p}_1 z = -\frac{1}{3} z + \frac{1}{3} + \frac{i}{3}, \ldots$

with $\boldsymbol{p}_j \begin{pmatrix} x_1 \\ x_2 \end{pmatrix} = \frac{1}{3} P_j \begin{pmatrix} x_1 \\ x_2 \end{pmatrix} + \frac{1}{3} p_j, \quad j = 0,1,\ldots 8$

The Peano curve: a complex representation

- Use ternary representation of $t \in I$:

$$0_3 t_1 t_2 \ldots t_{2n-2} t_{2n} \ldots = 0_9 (3t_1 + t_2)(3t_3 + t_4) \ldots (3t_{2n-1} + t_{2n}) \ldots$$

$$f_p(t) = \lim_{n \to \infty} \boldsymbol{p}_{3t_1 + t_2} \boldsymbol{p}_{3t_3 + t_4} \ldots \boldsymbol{p}_{3t_{2n-1} + t_{2n}} \Omega$$

- Continue as with Hilbert´s curve...

→ we get the same result as in Peano´s definition

Approximating polygons for the Peano curve

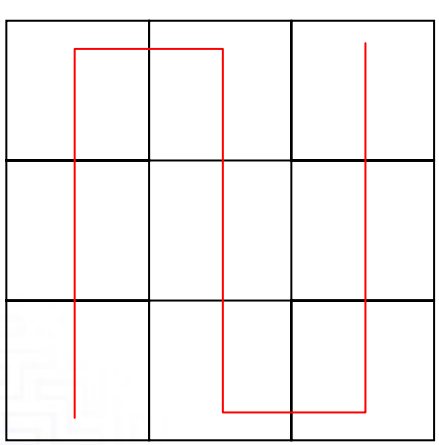

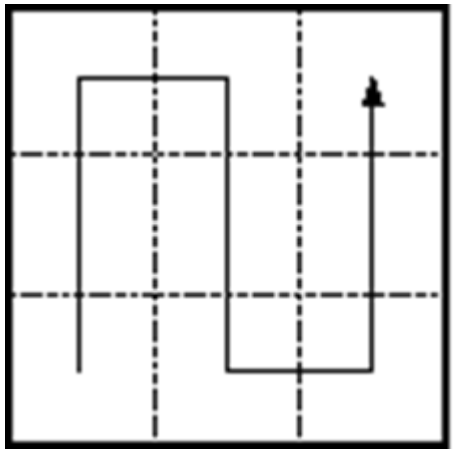

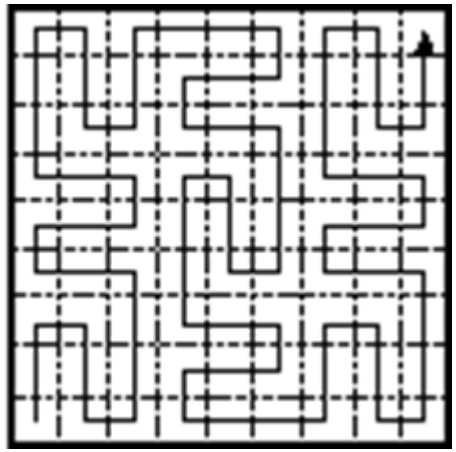

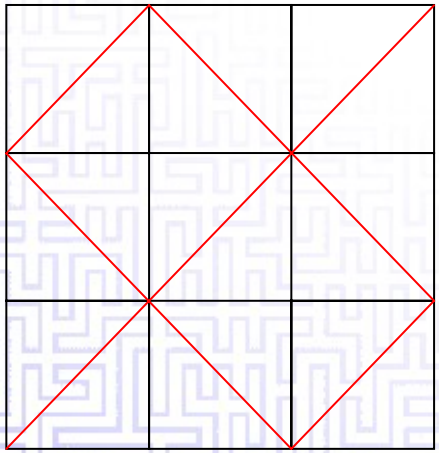

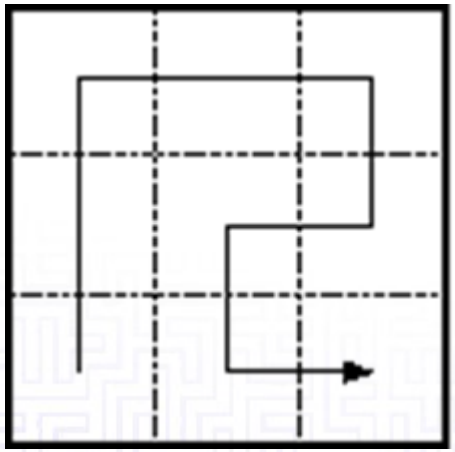

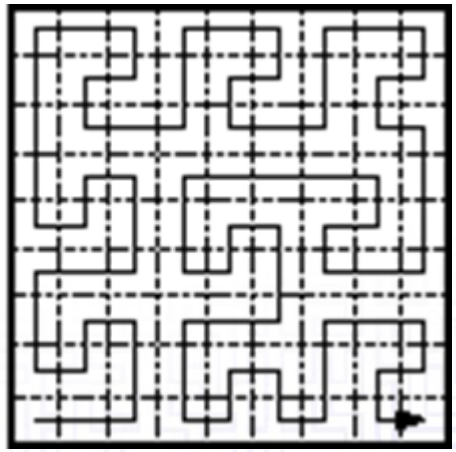

The Peano curve: representation through grammars

$$
\begin{aligned}
P &\longleftarrow P \uparrow Q \uparrow P \rightarrow S \downarrow R \downarrow S \rightarrow P \uparrow Q \uparrow P \\
Q &\longleftarrow Q \uparrow P \uparrow Q \leftarrow R \downarrow S \downarrow R \leftarrow Q \uparrow P \uparrow Q \\
R &\longleftarrow R \downarrow S \downarrow R \leftarrow Q \uparrow P \uparrow Q \leftarrow R \downarrow S \downarrow R \\
S &\longleftarrow S \downarrow R \downarrow S \rightarrow P \uparrow Q \uparrow P \rightarrow S \downarrow R \downarrow S
\end{aligned}
$$

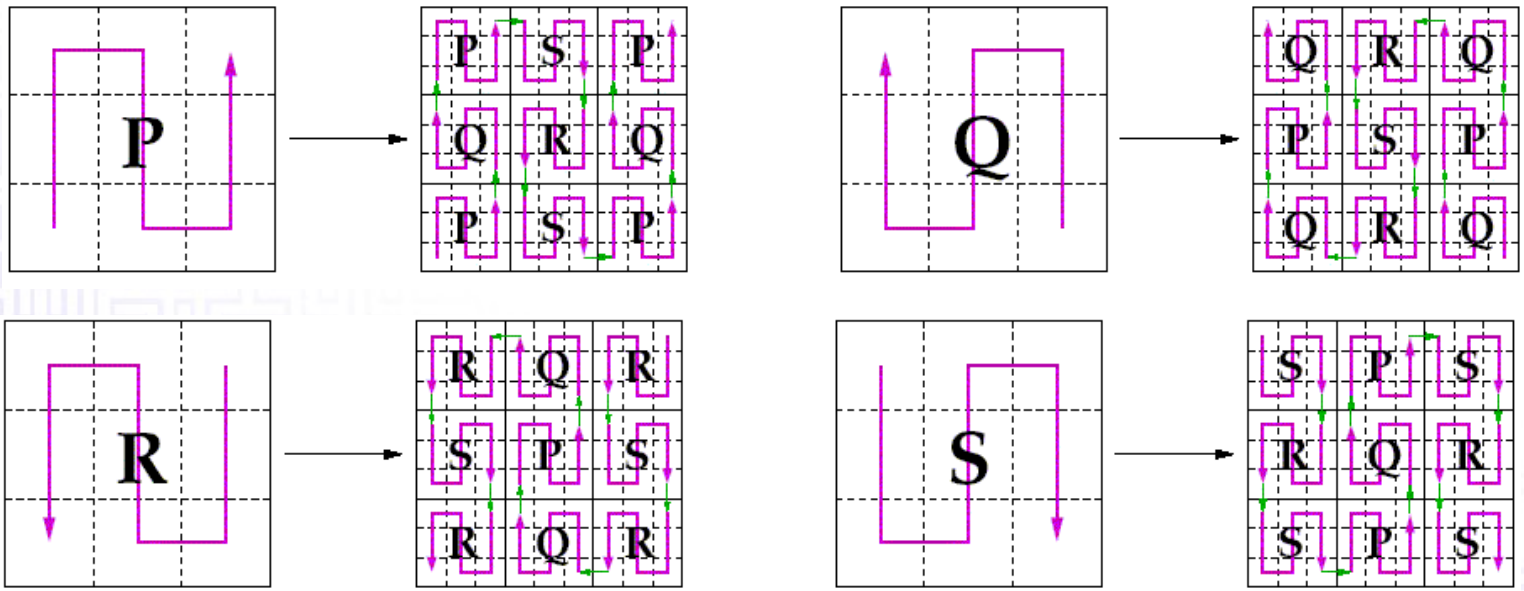

Contents

1. Introductory section
2. Types of space-filling curves
    1. The Hilbert space-filling curve
    2. The Peano space-filling curve
    3. The Sierpinski space-filling curve
    4. The Lebesgue space-filling curve
3. Application of space-filling curves

The Sierpinski curve: generation

- Partition *I* into 2^n congruent subintervals and τ into 2^n congruent subtriangles.

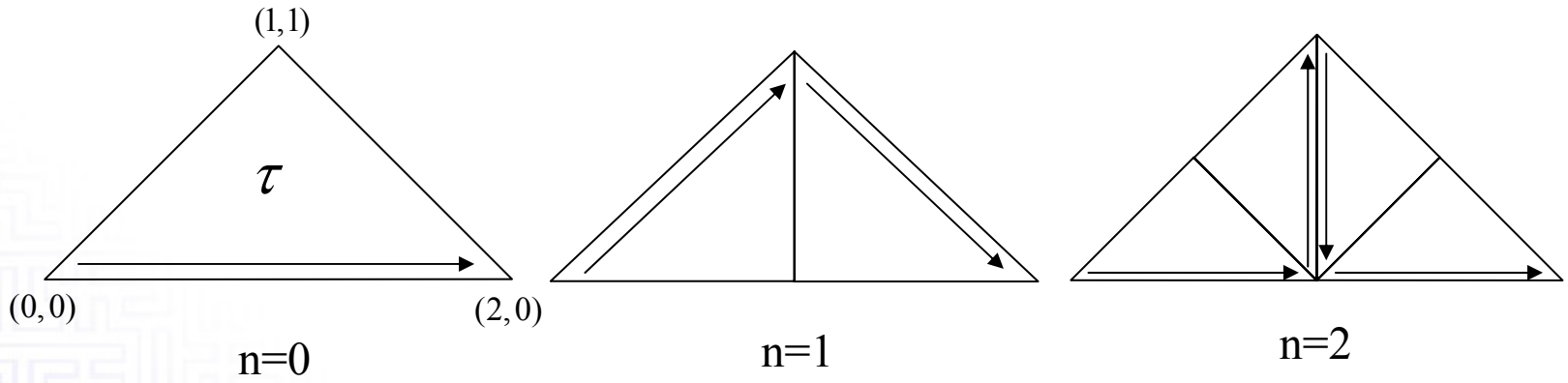

- In deriving an algabraic representation it is easier to divide *I* into 2^{2n} subintervals, thus using quaternaries:

$$f_s(0_4 q_1 q_2 q_3 \ldots) = \sum_{j=1}^{\infty} \frac{1}{2^j} S_{q_0} S_{q_1} S_{q_2} \ldots S_{q_{j-1}} s_{q_j}$$

The Sierpinski curve: generation

with similarity transforms:

$$\boldsymbol{S}_0 z = z/2 \qquad : \boldsymbol{S}_0 \begin{pmatrix} x_1 \\ x_2 \end{pmatrix} = \frac{1}{2}\begin{pmatrix} 1 & 0 \\ 0 & 1 \end{pmatrix}\begin{pmatrix} x_1 \\ x_2 \end{pmatrix} + \frac{1}{2}\begin{pmatrix} 0 \\ 0 \end{pmatrix} = \frac{1}{2} S_0 \begin{pmatrix} x_1 \\ x_2 \end{pmatrix} + \frac{1}{2} s_0$$

$$\boldsymbol{S}_1 z = zi/2 + 1 \qquad : \boldsymbol{S}_1 \begin{pmatrix} x_1 \\ x_2 \end{pmatrix} = \frac{1}{2}\begin{pmatrix} 0 & -1 \\ 1 & 0 \end{pmatrix}\begin{pmatrix} x_1 \\ x_2 \end{pmatrix} + \frac{1}{2}\begin{pmatrix} 2 \\ 0 \end{pmatrix} = \frac{1}{2} S_1 \begin{pmatrix} x_1 \\ x_2 \end{pmatrix} + \frac{1}{2} s_1$$

$$\boldsymbol{S}_2 z = -zi/2 + 1 + i \qquad : \boldsymbol{S}_2 \begin{pmatrix} x_1 \\ x_2 \end{pmatrix} = \frac{1}{2}\begin{pmatrix} 0 & 1 \\ -1 & 0 \end{pmatrix}\begin{pmatrix} x_1 \\ x_2 \end{pmatrix} + \frac{1}{2}\begin{pmatrix} 2 \\ 2 \end{pmatrix} = \frac{1}{2} S_2 \begin{pmatrix} x_1 \\ x_2 \end{pmatrix} + \frac{1}{2} s_2$$

$$\boldsymbol{S}_3 z = z/2 + 1 \qquad : \boldsymbol{S}_3 \begin{pmatrix} x_1 \\ x_2 \end{pmatrix} = \frac{1}{2}\begin{pmatrix} 1 & 0 \\ 0 & 1 \end{pmatrix}\begin{pmatrix} x_1 \\ x_2 \end{pmatrix} + \frac{1}{2}\begin{pmatrix} 2 \\ 0 \end{pmatrix} = \frac{1}{2} S_3 \begin{pmatrix} x_1 \\ x_2 \end{pmatrix} + \frac{1}{2} s_3$$

The Sierpinski curve: generation

- Taking into account some properties of S_{q_j} :

$$f_s(0_4 q_1 q_2 q_3 \ldots) = \sum_{j=1}^{\infty} \frac{1}{2^j} (-1)^{\eta_j} S^{\delta_j} s_{q_j}$$

with η_j = *number of* 2′*s preceding* $q_j \pmod 2$

and δ_j = *number of* 1′*s and* 2′*s preceding* $q_j \pmod 4$

The Sierpinski curve: approximating polygons

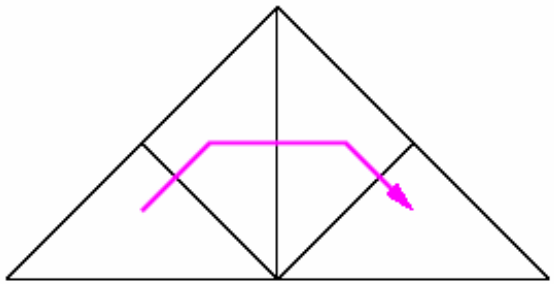

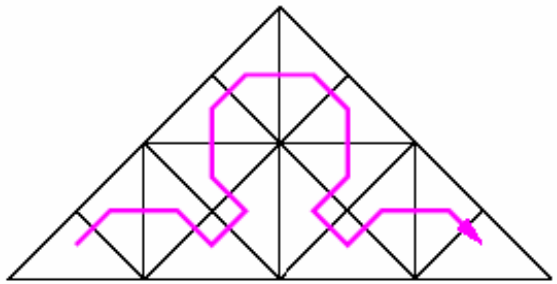

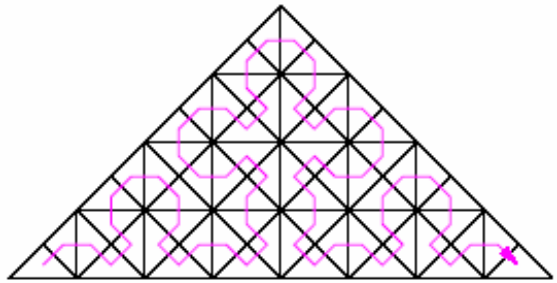

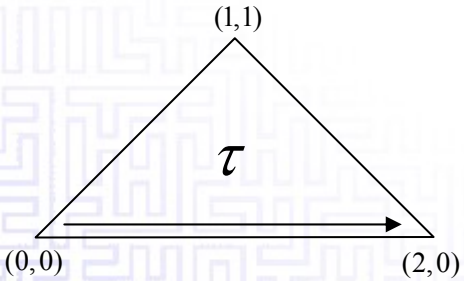

n=0

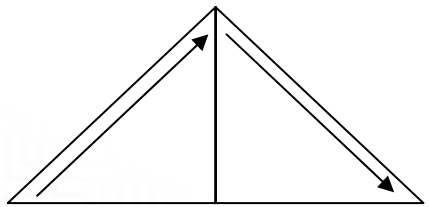

n=1

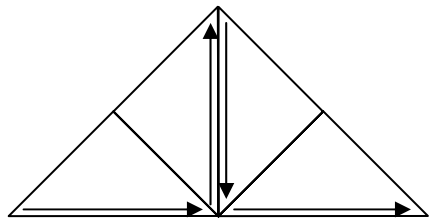

n=2

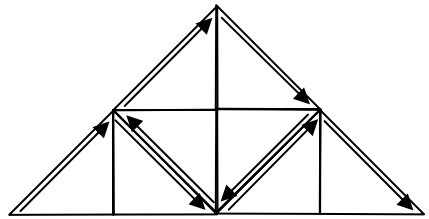

n=3

The Sierpinski curve: generation

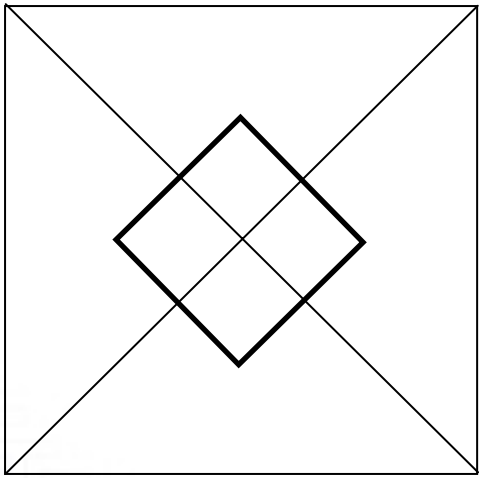

Originaly defined as a map f_s from *I* onto $[-1,1]^2$ but it can be considered as a map from *I* onto a right isosceles triangle τ .

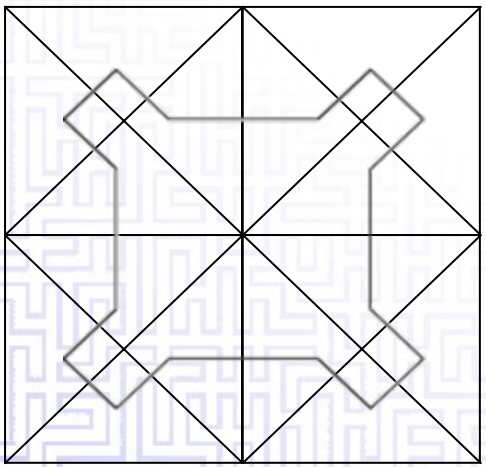

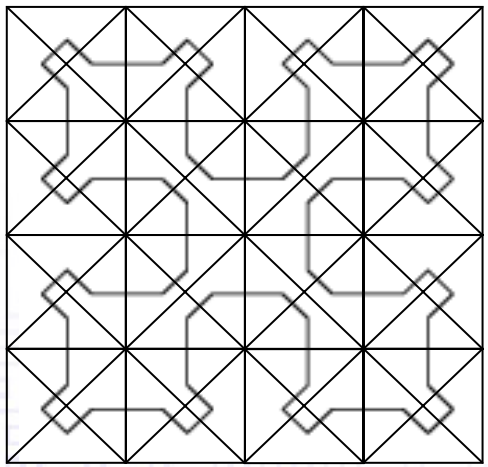

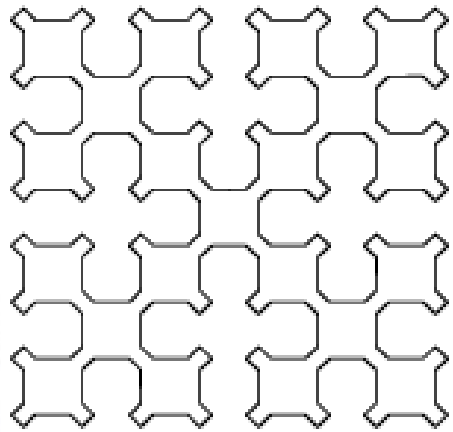

Contents

1. Introductory section
2. Types of space-filling curves
    1. The Hilbert space-filling curve
    2. The Peano space-filling curve
    3. The Sierpinski space-filling curve
    4. The Lebesgue space-filling curve
3. Application of space-filling curves

The Lebesgue curve: generation and approximating polygons

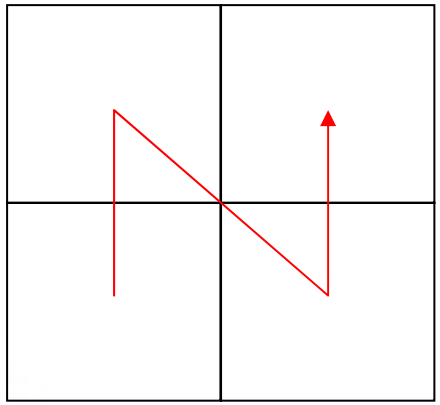

1st iteration

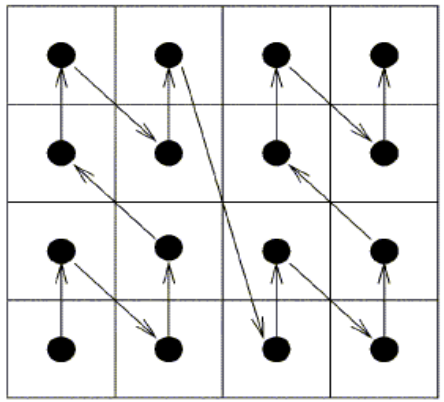

2nd iteration

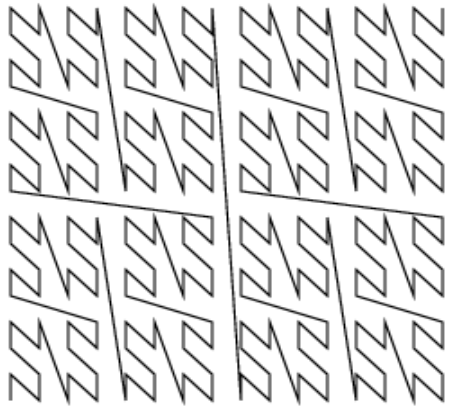

4th iteration

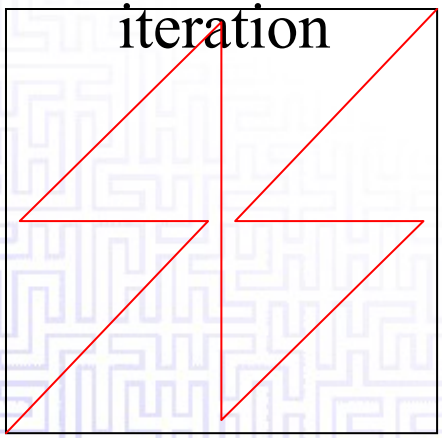

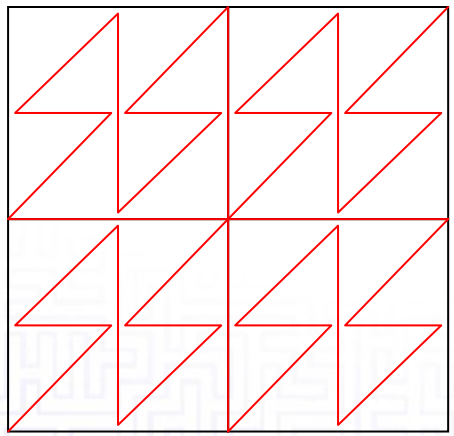

What can we do with Space-filling curves ?

Peano

&

Hilbert

Are these iterates of any use in engineering practice?

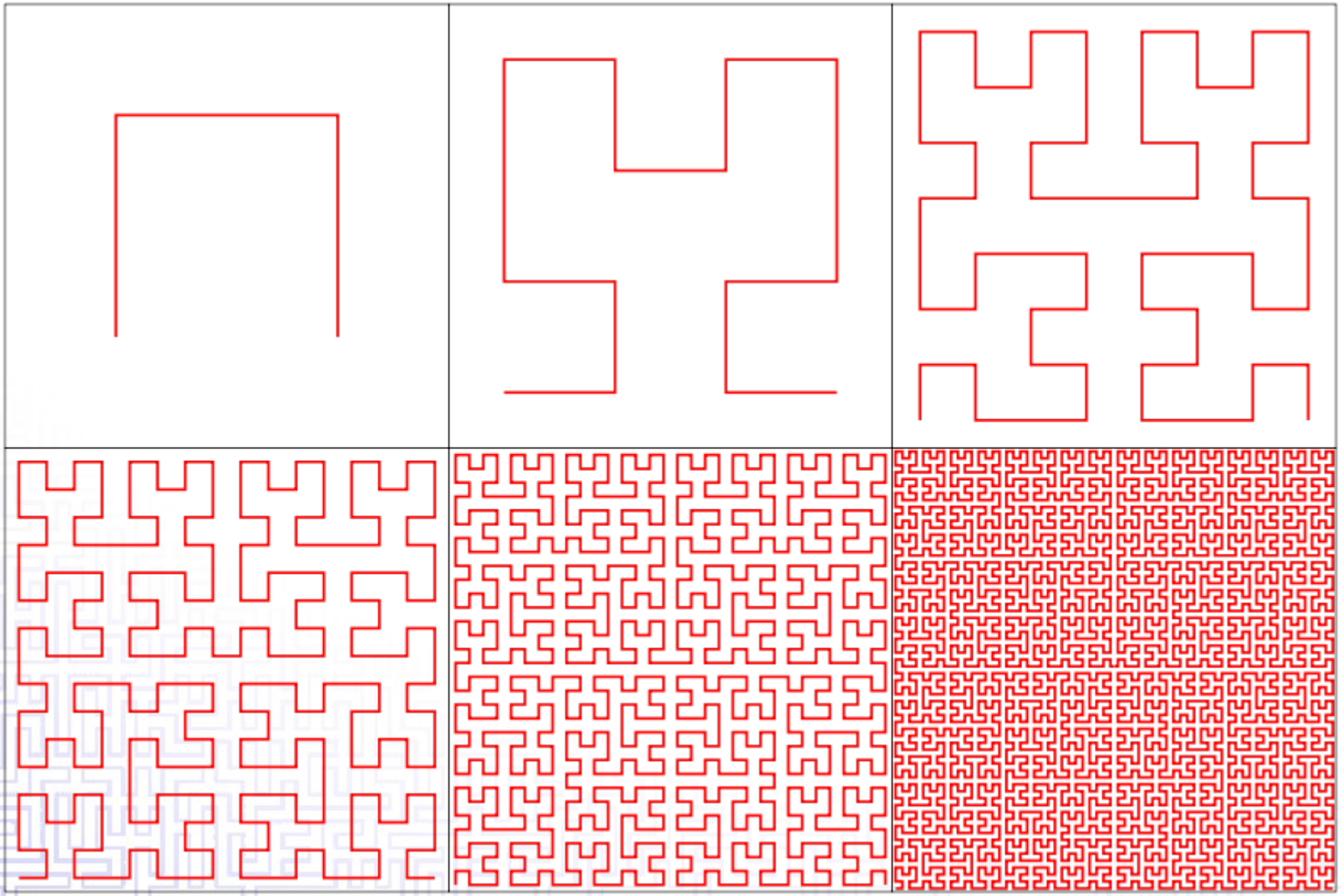

Fractal Square Loop Antennas

Main Benefit: Decreased Size

Decreased Antenna Width
Accompanies Increases in Iteration
For Second and Third Iteration

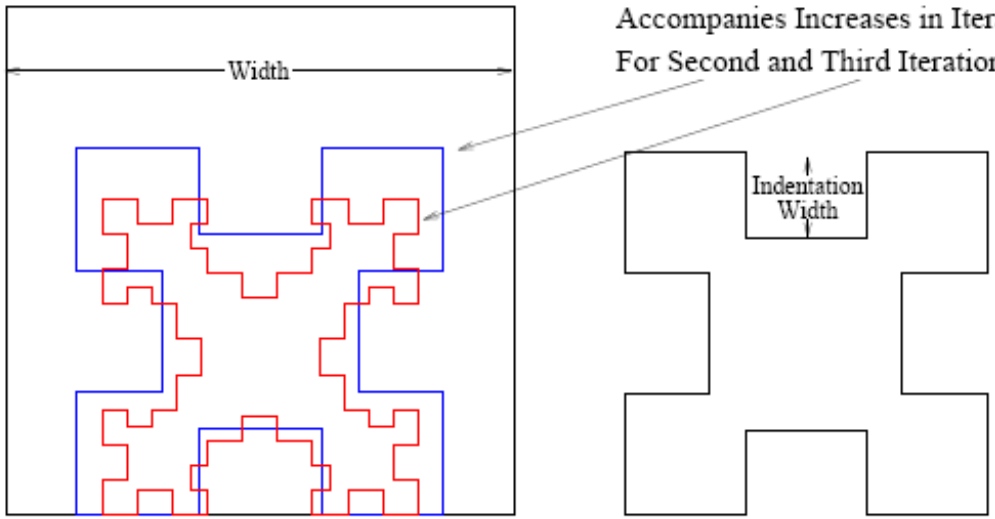

Far Field Pattern

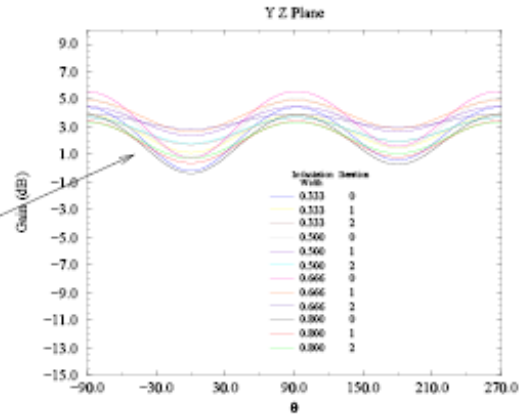

Far Field Pattern
Remains Similar
even with
Smaller Area

Fractal Antennas

Fractal Square Loop Antenna Design Curves

The Antenna can be Fabricated for a Given Iteration

$$Width = \frac{C}{e^{2*1.1}-1}$$

For a given indentation width, resonant loops can be designed using the above equation, where C is found empirically.

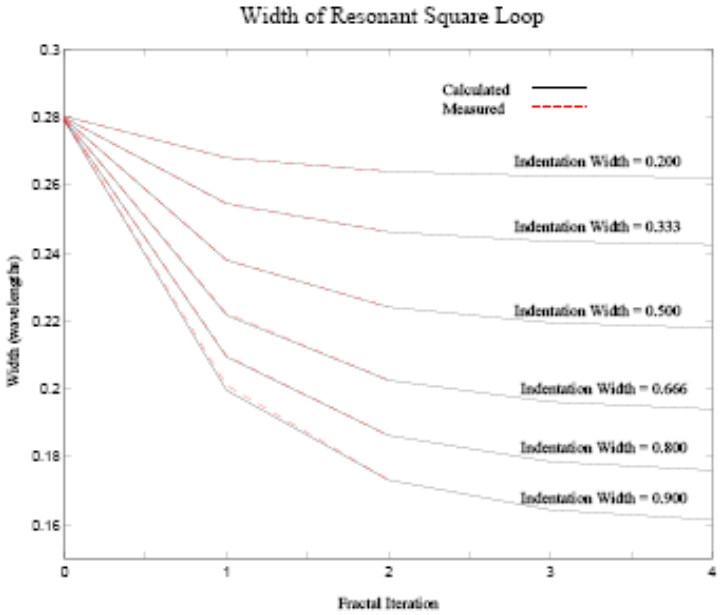

Fractal Antennas

Arrays with Fractal Elements

Main Benefit: Decreases Mutual Coupling between Elements

Separation Distance can be Maximized Using Fractal Elements

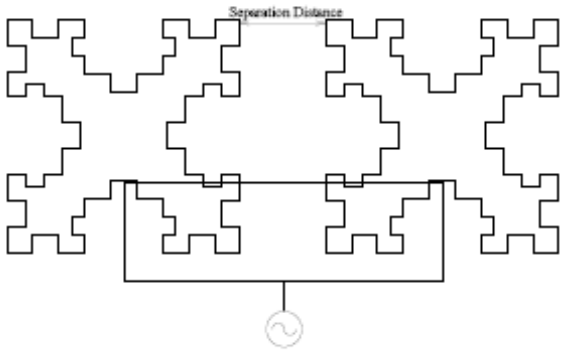

Thin Feeding Network for Fractal Array Elements

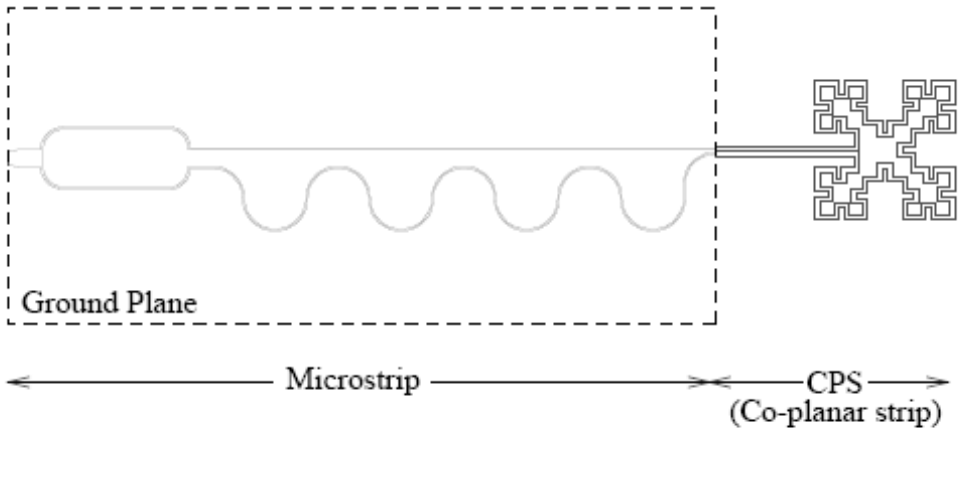

Fractal Antennas

John Gianvittorio - UCLA

Fabricated Fractal Array Antennas

Decreased inter-element coupling for fixed spacing
Increased packing ability with smaller fractal elements

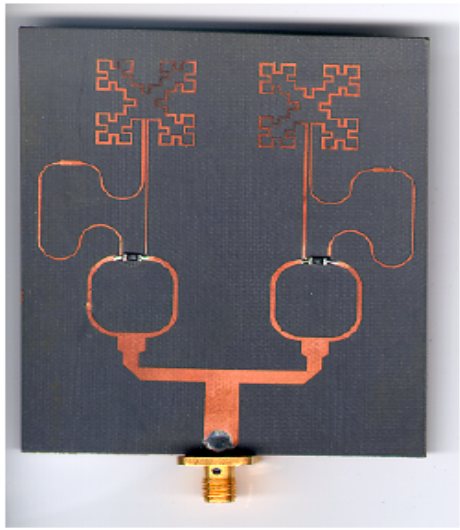

Fractal Array

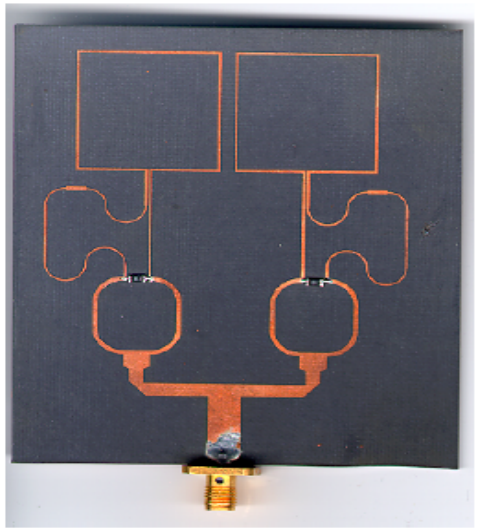

Standard Array

Fractal Antennas

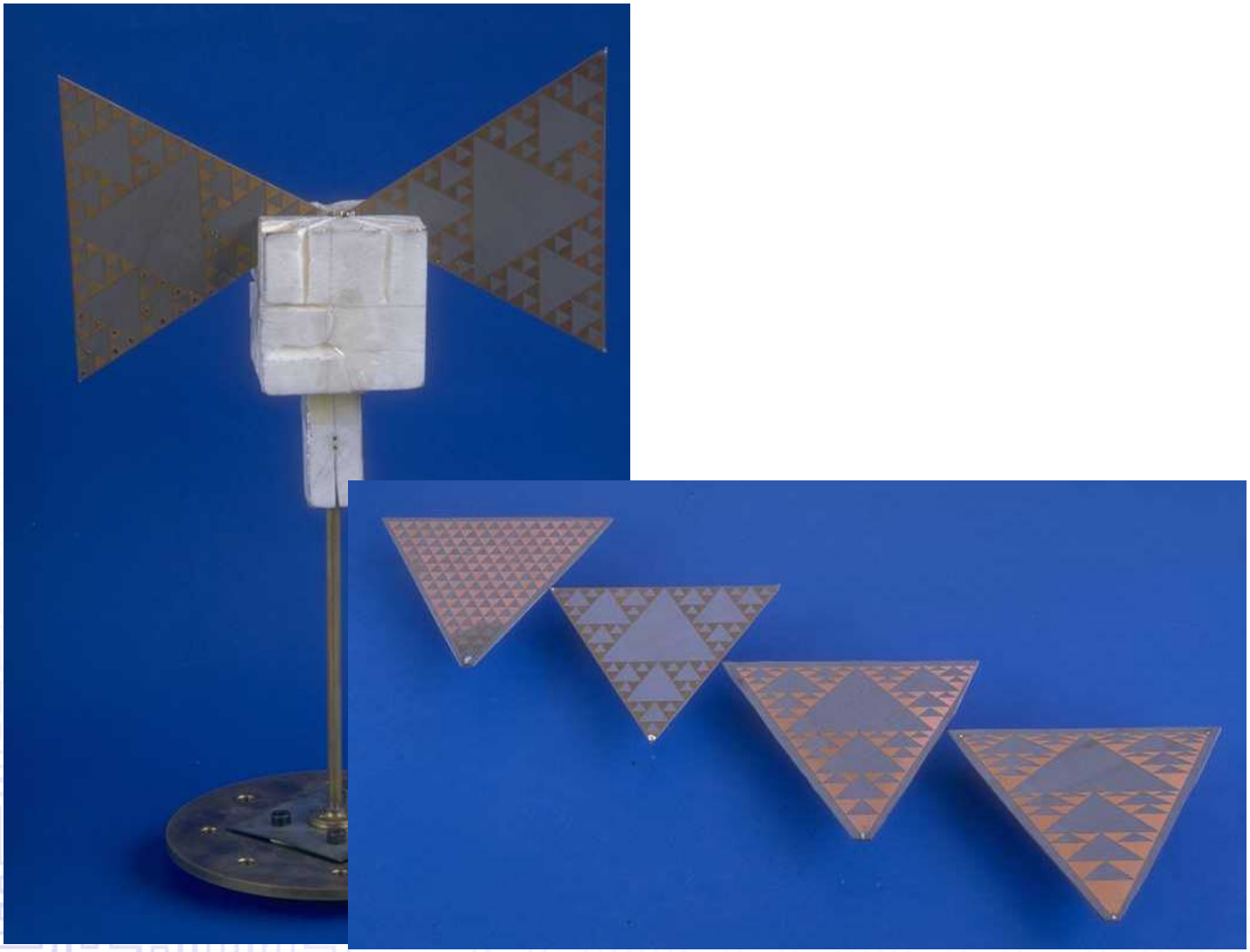

Fractal antenna design

- Sample fractal antenna elements:

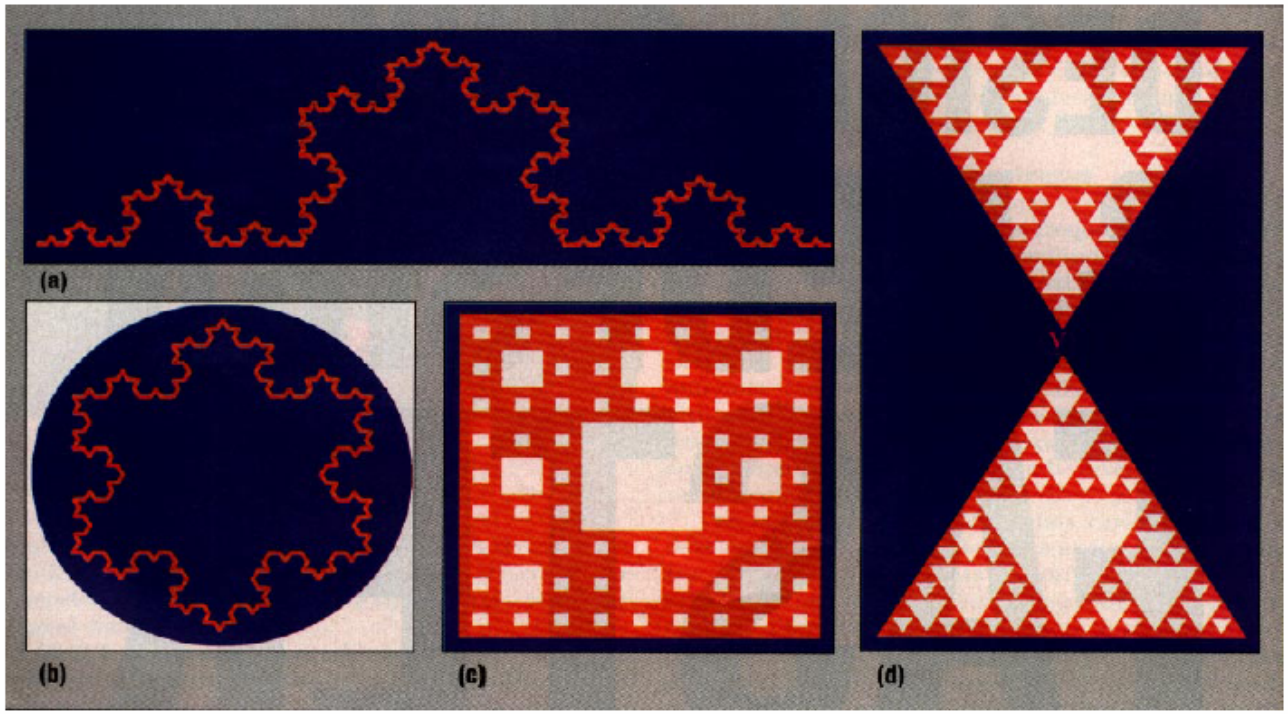

(a) Koch dipole **(b)** Koch loop **(c)** Cantor slot patch **(d)** Sierpinski dipole

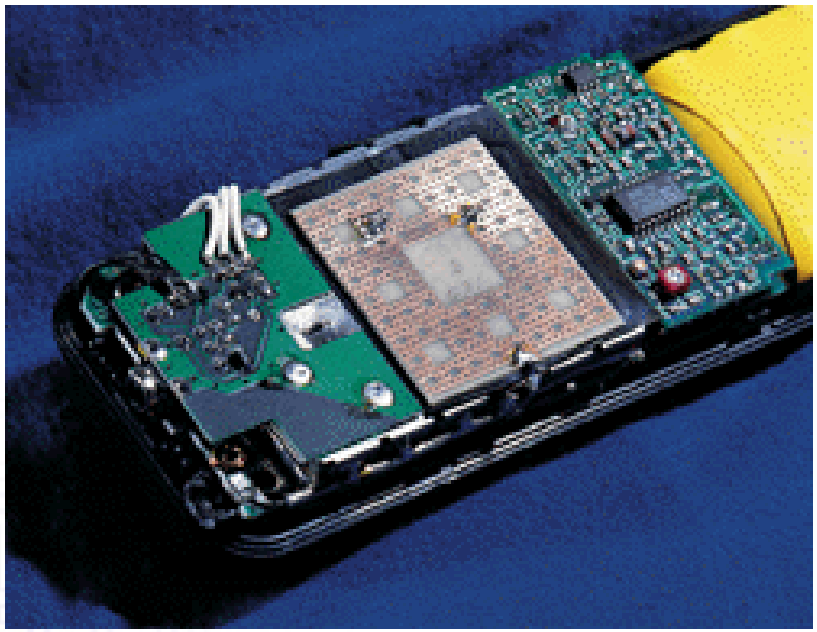

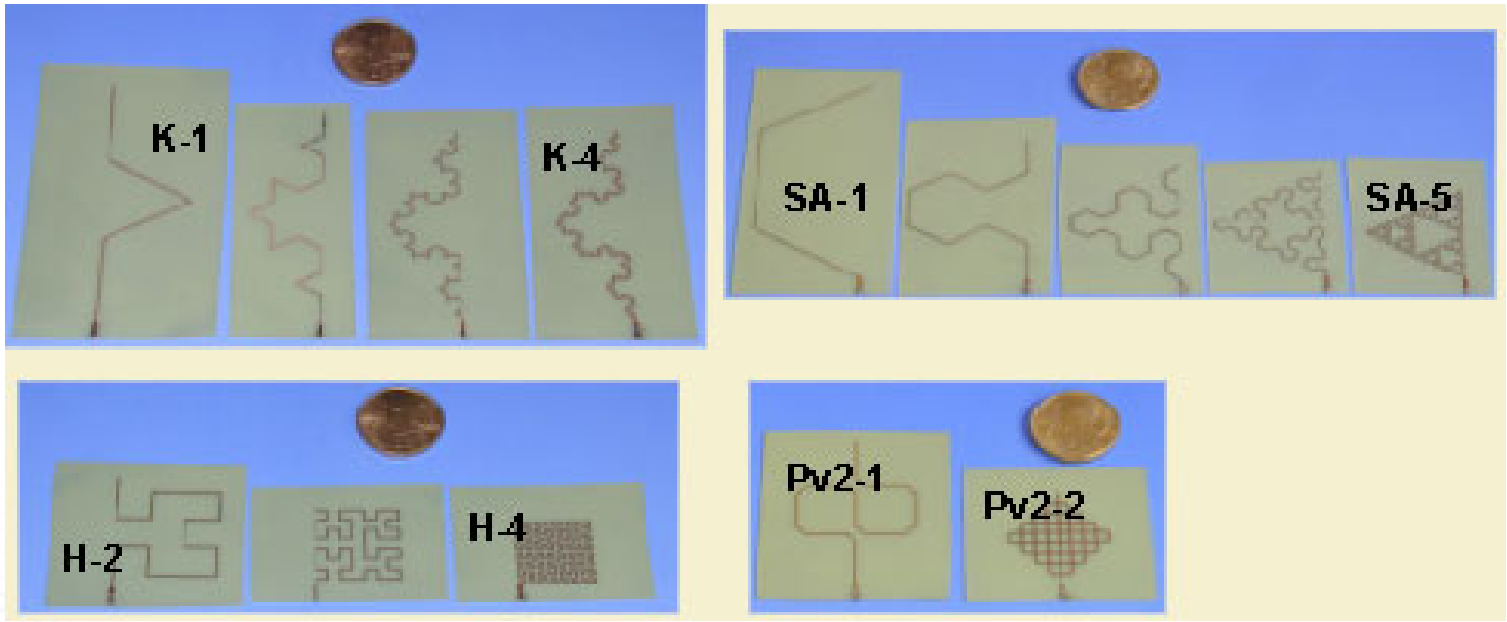

Printed monopoles used for the investigation on the influence of fractal dimension on radiation efficiency and quality factor. From left to right and top to bottom: Koch monopoles, Sierpinski Arrowhead monopoles, Hilbert monopoles and Peano variant 2 monopoles.

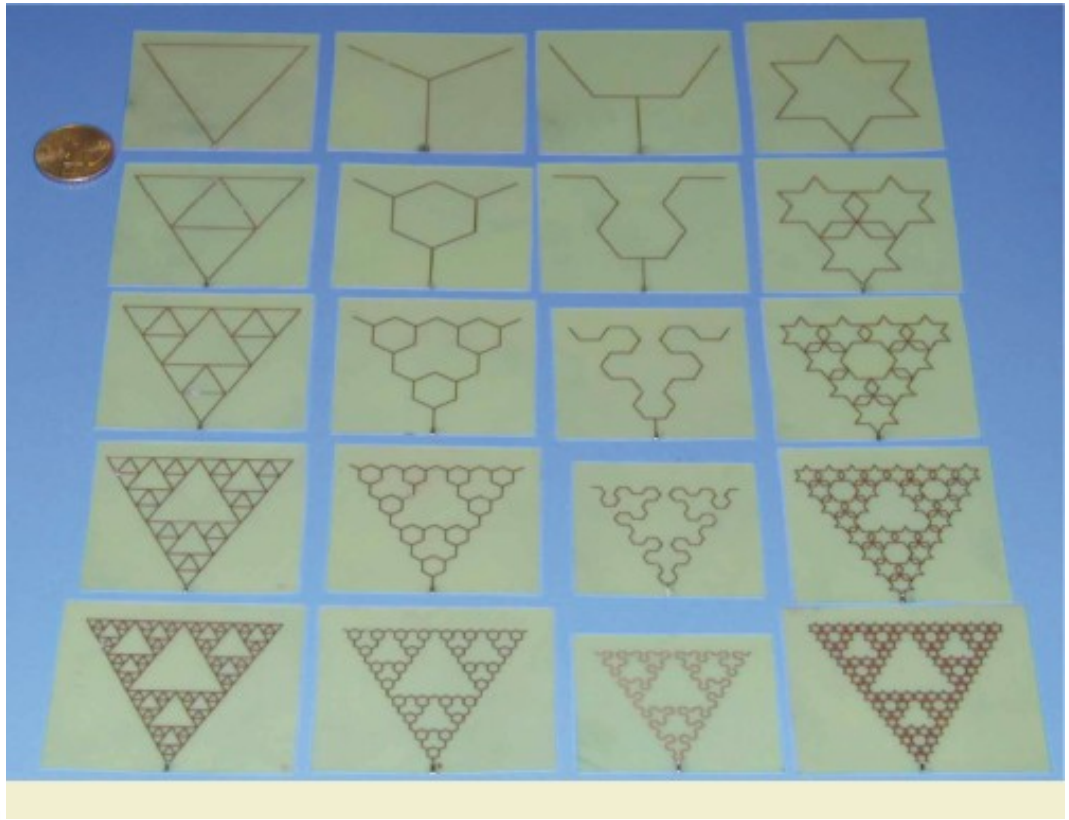

Manufactured prefractals with fractal dimension 1.58 compared with the size of 10 euro cents. From left to right and by columns: Delta-Wired Sierpinski monopoles (DWS); Y-Wired Sierpinski monopoles (YWS); Sierpinski Arrowhead monopoles (SA); and Koch-1 Sierpinski monopoles (K1S).

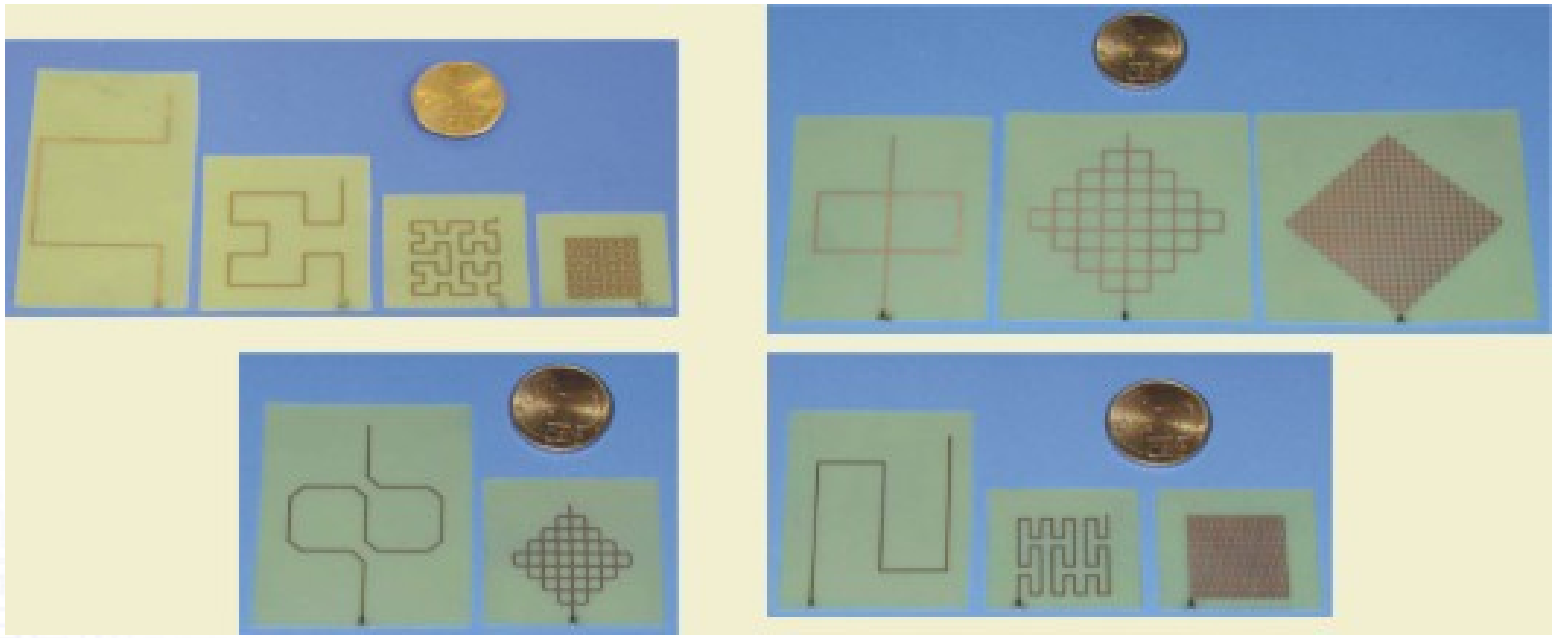

Manufactured prefractals with fractal dimension 2. From left to right and top to bottom: Hilbert monopoles (H); Peano monopoles (P); Peano variant 2 monopoles (Pv2) and Peano variant 3 monopoles (Pv3).

Put the Antenna in the Package

- The next major opportunity for wireless component manufacturers is to put the antenna into the package. Fractal-technology applied to antennas reaches the required miniaturisaton to make Full Wireless System in Package (FWSiP) a reality.
  - FracWaveTM technology
  - FracWaveTM Antenna in Package (AiP) technology is suitable for Bluetooth®, WLAN, GPS, UWB and Zigbee and for sensors for automotive, biomedical and industrial purposes.

Visualization of antenna (the brown layer) integrated on a package substrate

AiP integrated on Bluetooth® adapter

Fractus® Julia-12 ISM 2.4 GHz VPol

P/N: FR03-02-N-0-002

The **JULIA-12 ISM 2.4 GHz panel antenna** is a cost effective solution with an excellent broad coverage in a tiny package. The antenna features an internal Fractal shaped element and is suitable for both indoor and outdoor aplications.

Frequency Range	2.4 - 2.5 GHz
Directivity/Gain	9.6 dBi / 8.8 dBi
Impedance	50 Ω
Polarisation	VPOL
F/B Ratio	> 18 dB
VSWR	< 1.5 : 1
Vertical Beamwith	65°
Horizontal Beamwith	70°
Connector (Pig Tail)	RP-TNC or RP-SMA
Radome	ABS
Dimensions	10 x 10 x 3 cm

Measured results from a standard

Patent Pending: WO0154225, WO0122528, PCT/EP01/10589, PCT/EP02/07837, US60/613394, US60/627653 and PCT/EP02/07836

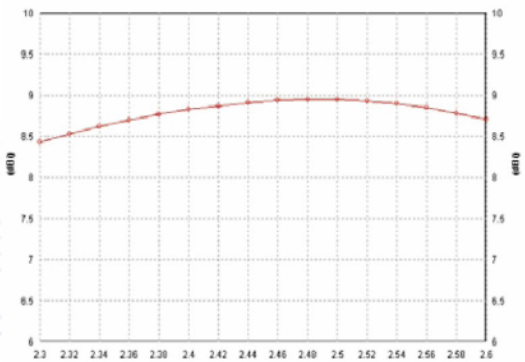

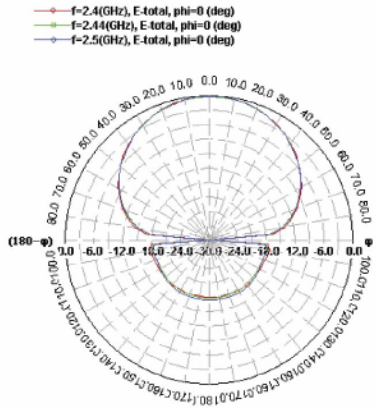

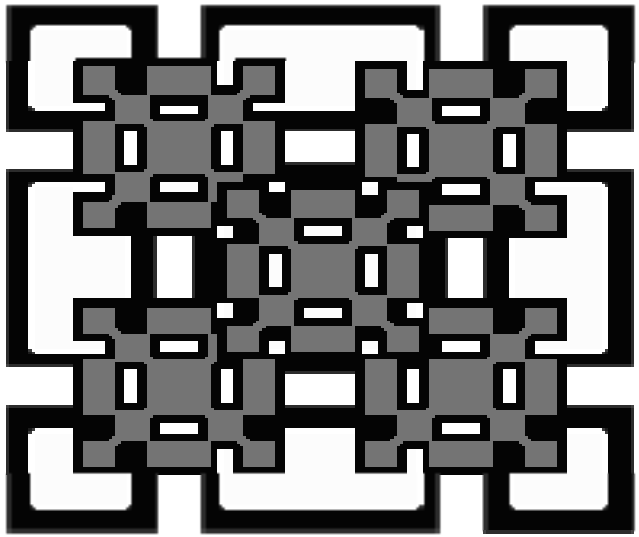

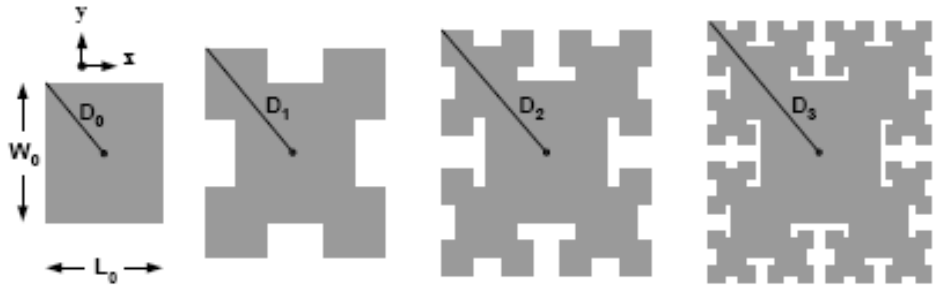

Figure 1. Construction of the Fractal Rectangular Curve (FRC), a) FRC0 (Initiator), b) FRC1, c) FRC2, d) FRC3.

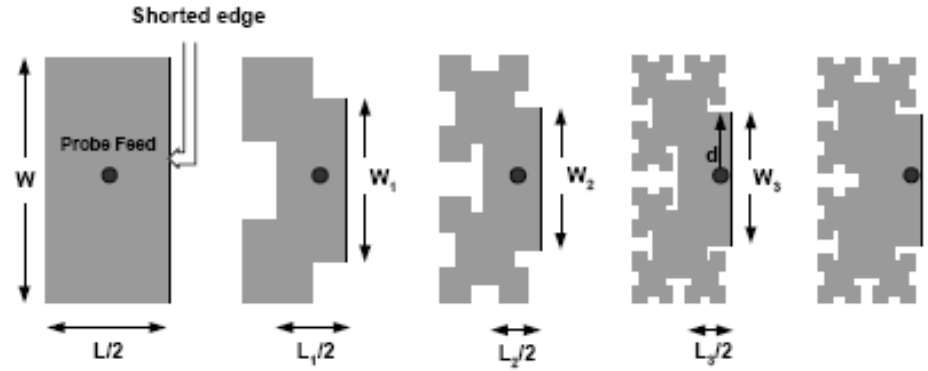

Figure 2. Geometry of the Simulated Shorted Elements, a) S-FRC0, b) S-FRC1, c) S-FRC2, d) S-FRC3 and e) Modified S-FRC3 (MS-FRC3).

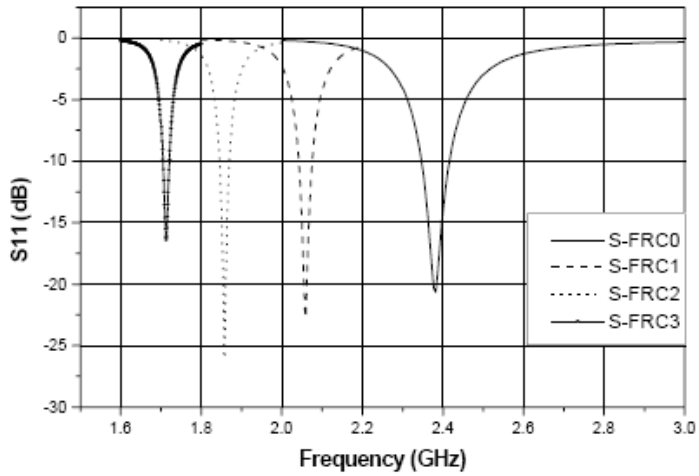

Figure 3. Simulated input return losses (S11) of the S-FRCs.

TABLE 1. SIMULATED RESONANCE PERFORMANCE

Antenna	f_n (GHz)	BW_n (%)	$(f_n-f_0)/f_n$(%)	n (%)
S-FRC0	2.381	2.90	--	39.4
S-FRC1	2.059	1.75	13.5	37.2
S-FRC2	1.858	1.34	22.0	33.2
S-FRC3	1.713	0.93	28.0	30.0

After „Reduced Size Fractal Rectangular Curve Patch Antenna" by G. Tsachtsiris, C. Soras, M. Karaboikis and V. Makios

Limitations

Fractal electrodynamics analysis

Some History

- 40's. *L.J.Chu* and *H.Wheeler* stablish a **fundamental limit** on the performance of **small antennas**.
- 60's. Several research teams at the *University of Illinois at Urbana-Champaign*, *University of California* and *Ohio State University* introduce the concept of **frequency-independent antennas**. The self-scaling concept gives place to the **log-periodic dipole array** and to the **spiral antennas**.
- 70's. *B. Mandelbrot* coins the term '**Fractal**'. Such a name is used to describe a family of geometrical objects that defy the traditional rules of the Euclidean geometry. Later on, Mandelbrot states that such a weird fractal shapes are, in fact, among the most common forms in nature.
- 80's. *D.Jaggard et al*. coin the term '**Fractal Electrodynamics**'. **Electromagnetics** and **Fractal Geometry** blend into a novel discipline. The **interaction** of fractal bodies and electromagnetic waves are investigated and some relationships between common **fractal properties** and the scattered electromagnetic waves are stablished.
- 90's. The first reported **fractal multiband antennas** are introduced by *C.Puente et al.* from the *Universitat Politècnica de Catalunya*. Also, the potentiallity of fractals to become **small antennas** is introduced by *N.Cohen* from the *University of Boston*.

- L. J. Chu, “Physical limitations on omni-directional antennas,” *J. Appl.Phys.*, vol. 19, pp. 1163–1175, 1948.

1. H.A.Wheeler, "**Fundamental Limitations of Small Antennas**," Proc. IRE, pp. 1479-1488. December, 1947.

- D.L.Jaggard, "**On Fractal Electrodynamics**," in Recent Advances in Electromagnetic Theory, pp. 183-224, D.L.Jaggard and H.N.Kritikos, Editors; Springer Verlag, 1990

Fractal electrodynamics

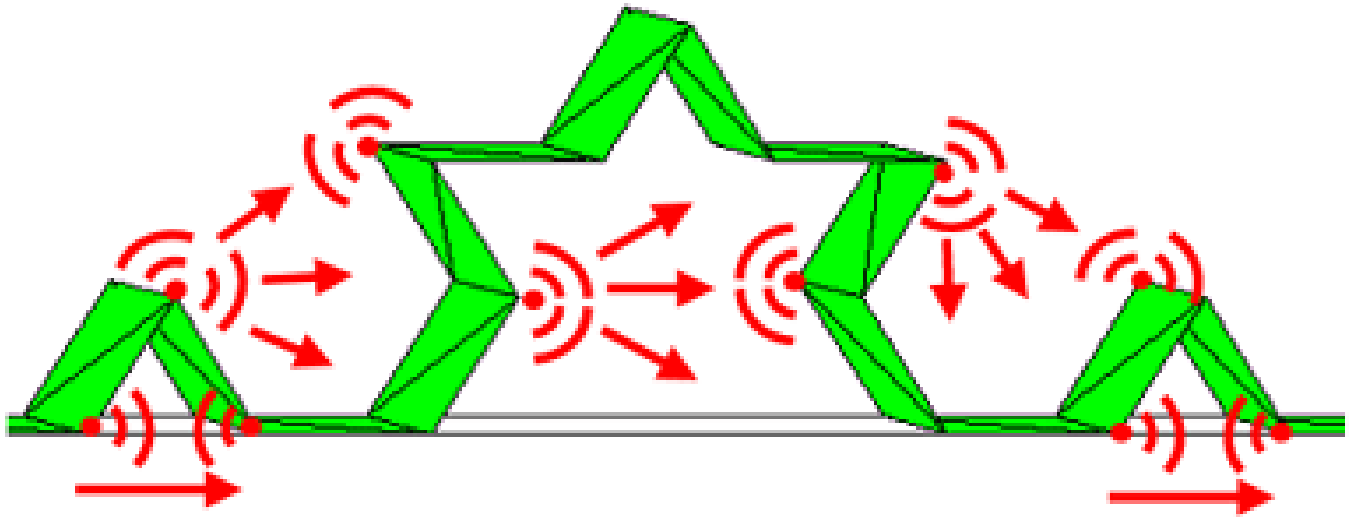

The angles radiate a spherical wave with phase center at the vertex. Each angle not only radiates, but also receives the signal radiated by other angles. As a consequence, part of the signal does not follow the wire path, but takes “shortcuts” that start at a radiating angle. The length of the path traveled by the signal is, therefore, shorter than the total wire length. The higher iteration number in the Koch antenna, the more angles it has and the closer to each other they are, so the more signal takes shortcuts and the less signal follows the whole curve path.

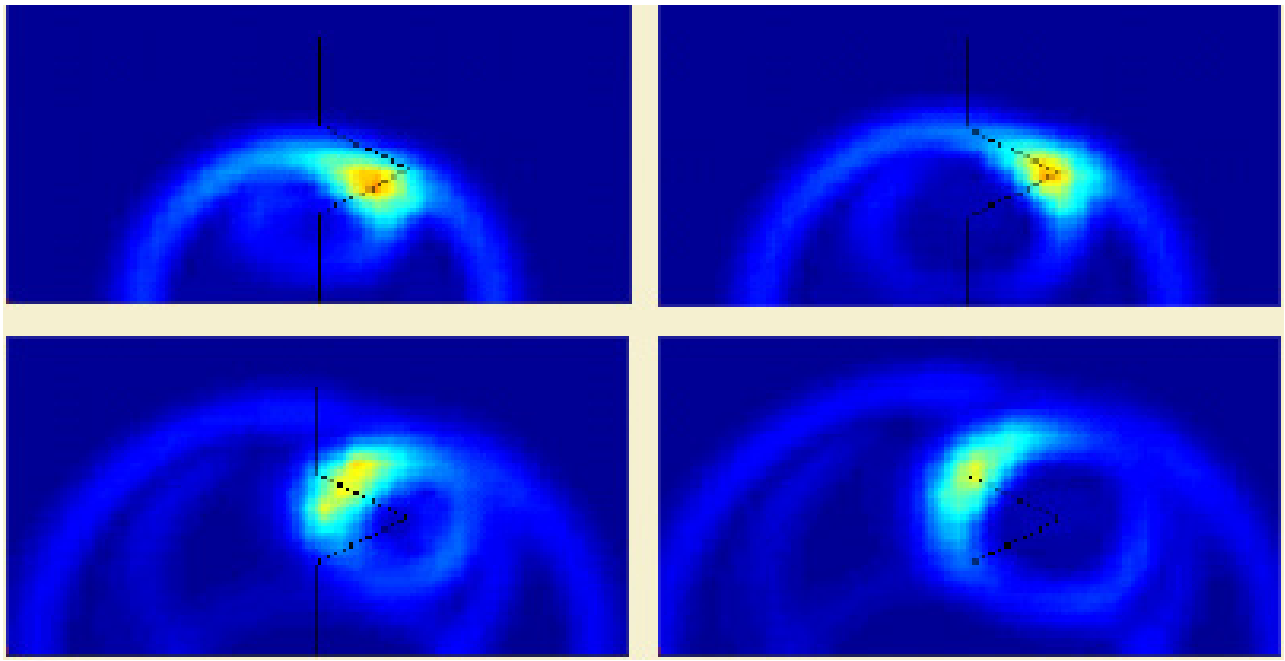

Near fields in the time domain in the vicinity of a single-iteration Koch monopole (K1) with short-pulse excitation. The sharp angles of the pre-fractal curve become the center of spherical wave radiation, which corroborates the coupling or shortcut effect hypothesis.

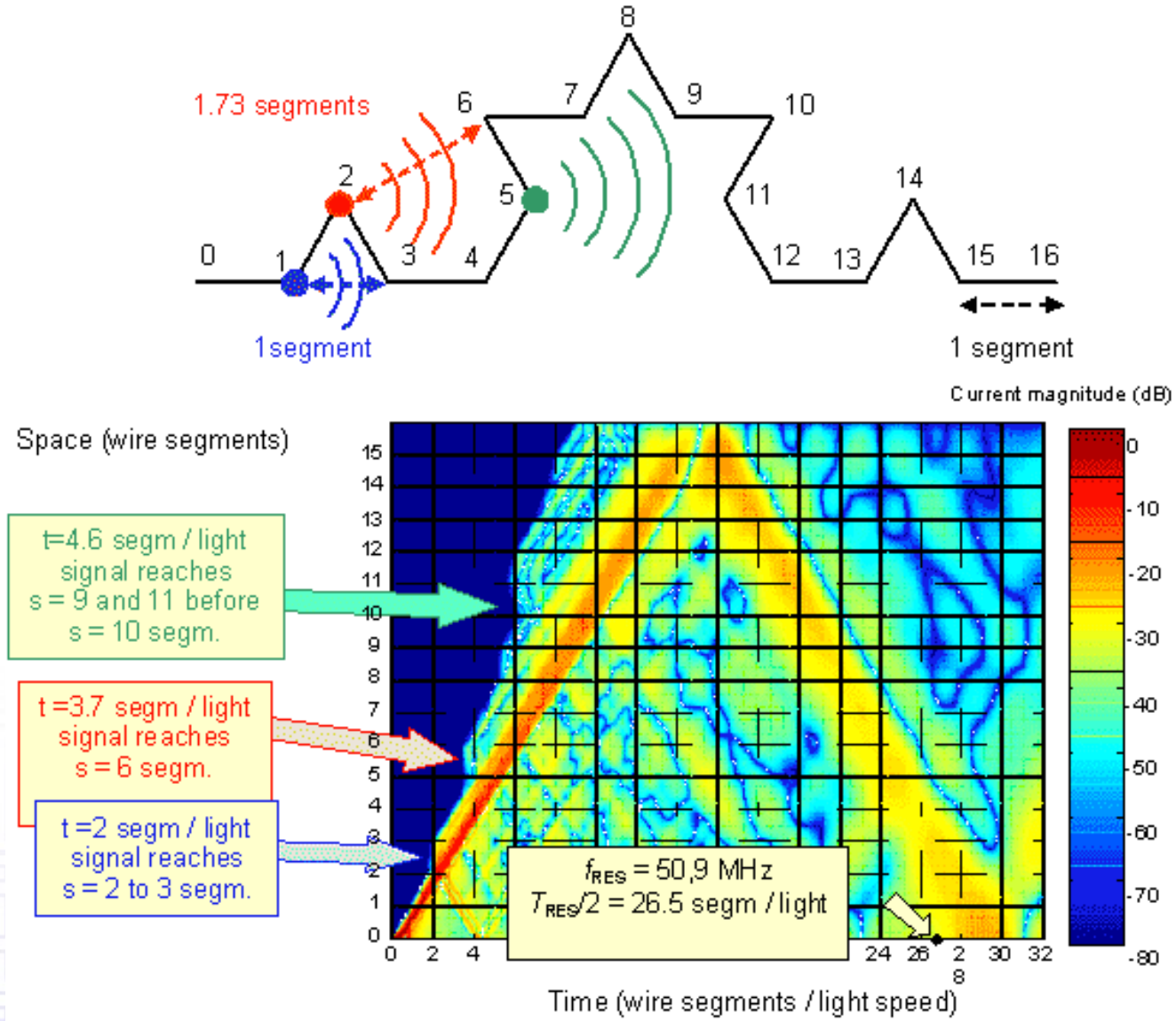

*Figure 7: Space time-diagram for short-pulse excitation in a 1m-height K2 monopole. The antenna has been modeled as a thin wire using DOTIG code from University of Granada. The signal shortcuts from angles 1 to 3 (**blue** color), 2 to 6 (**red** color) and 5 to 9 (**green** color) can be clearly observed*

- Increasing the number of iterations means a reduction on resonant frequency, radiation efficiency and an increase on quality factor. The increase of **fractal dimension**, although making better space filling curves, builds larger monopoles with lower efficiencies and higher quality factors even for the first iterations.
- **Topology** has a stronger influence than fractal dimension on the behaviour of small 2D pre-fractal wire monopoles, in particular on the losses efficiency.
- As the **number of loops** inside the structure increases, efficiency and fractional bandwidth (inverse of quality factor) seem to increase with the order of the pre-fractal (number of IFS iterations).

- When there is **no loop**, each iteration increases the length and bending of the wires, and as a consequence ohmic losses and the amount of stored energy on the surrounding of the antenna increases (this means lower radiation efficiencies and higher quality factors).
- When the number of iterations increases beyond a certain threshold, the change in radiation patterns and input impedance of the antenna tend to zero. In other words, **there is no use in increasing the number of iterations**. Convergence is usually achieved between 4 and 6 iterations. This value depends largely on the size, wire or strip width and topology of the antenna.

- The hypothesis of **electromagnetic coupling** –or shortcuts- between corners fully explains why the resonant frequency of pre-fractal antennas is much larger than what could be expected from the wire length only and why it stagnates as the number of iterations increases.
- It seems that the **high-gain localized modes** that have been previously observed in the Koch-island printed patch antenna are **not exclusive of pre-fractal antennas**.
- **Three-dimensional** design does not provide further improvements over planar design in the radiation performance of monopoles. In spite of the smaller electrical sizes attainable thanks to their increased space-filling capability, they have a more intricate topology and larger wires than their planar counterparts. Consequently, efficiency and Q factor for these 3D pre-fractals have unpractical values to real-world applications.

Some guidelines

- In order to reduce signal coupling –or shortcuts- between wire segment angles, the distance between those angles must be as large as possible, and the angles the larger possible.
- In order to reduce the signal coupling between the feeder and the wire segments, the most possible wire length must be perpendicular to the electric field radiated by the feeder.
- In order to reduce coupling between wire segments, parallel wire segments with opposite (anti-parallel) currents very close to each other must be avoided.
- An example of wire antenna that closely follows these guidelines is a **two-arm square spiral**. The resonant frequency of a square spiral is inversely proportional to the wire length, while keeping the wire enclosed by a small square.

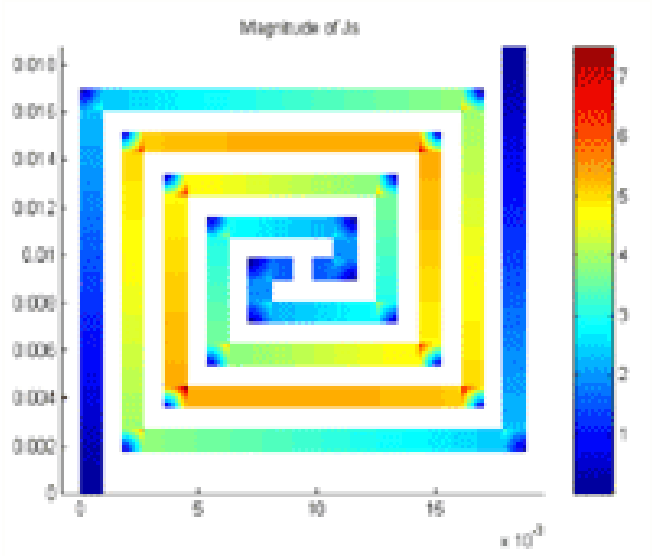

	Resonant freq. [GHz]
Spiral 4-turns	1.77
Straight dipole unwrapped spiral	1.6
Straight dipole diagonal	11.6

Resonant frequency of a 4-turn two-arm spiral, the straight monopole of equal length and the longer monopole that would fit in the reference square

Taking as working surface a square of side SL=1.875cm, different iterations of a spiral have been studied and compared with two straight dipole configurations: the dipole of length equal to the unwrapped spiral length and the longer dipole that would fit in the reference square, having as length the diagonal of the square. Table shows that the spiral antenna has a resonant frequency almost as low as the straight dipole of same wire length. According to the guidelines derived from the shortcuts or couplings study in preceding section, this is due to the weak electromagnetic coupling between angles, between the feeder and the strip or between parallel strip segments with opposite current. Unlike pre-fractal antennas, the resonant frequency scales almost linearly with the inverse of strip length while keeping the wire enclosed by a small square. The spiral antenna constitutes a very good benchmark to judge pre-fractal antennas as provides a tough challenge offering excellent miniaturization while keeping a reasonable frequency behaviour

Other applications of space-filling curves

2 dimensional SFCs give a recipe for going through a set of 2 dimensional data that are arranged on a grid:

- going through pixels that make up an image being scanned
- matrix operations in linear algebra
- going through / representing a 2D computational grid
- ...

Favorable property: better exploitation of the 2D locality due to the recursive nature / self-similarity.

Application of space-filling curves

1. Representation of computational grids (1)

Acceptable computational complexity is required in implemen-ting computational grids. Especially for adaptively refined grids the manipulation part cannot be too expensive → choice of ap-propriate data structures is important.

Often applied: space trees of which the leaves correspond to the grid cells that are enumerated by a discrete SFC. For adaptively refined grids we use different iterates depending on the level of refinement.

Application of space-filling curves

1. Representation of computational grids (2)

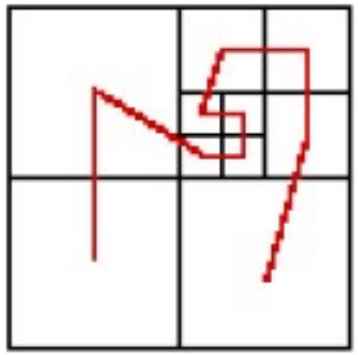

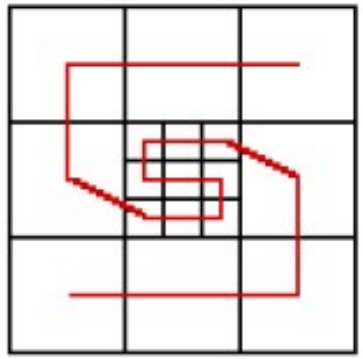

Application of space-filling curves

2. Implementation with respect to cache-efficiency (1)

- Data access of hierarchically stored data can be slow. By using SFC we try to process the data linearly in a way that reduces data access time and cache misses.

- Build a fixed number of stacks to avoid random access in the memory, such that data (information in a grid point) needed in the operation sequence is always on top. The corresponding processing order of the grid cells is defined by a SFC.

Application of space-filling curves

2. Implementation with respect to cache-efficiency (2)

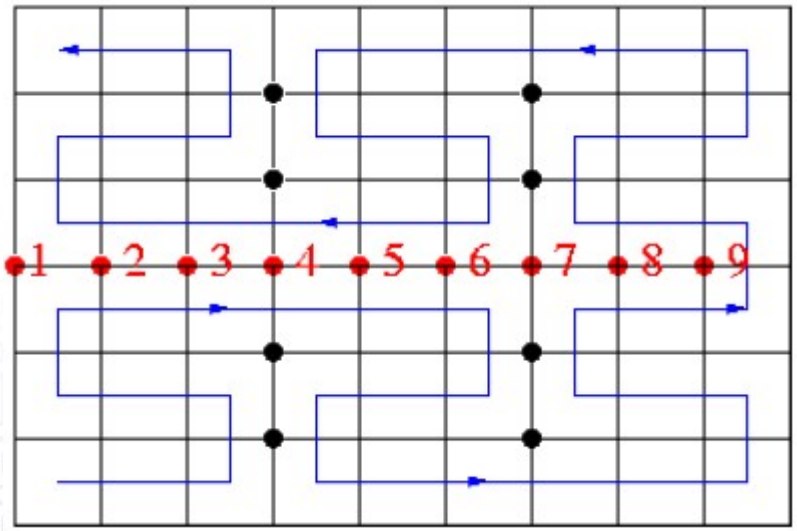

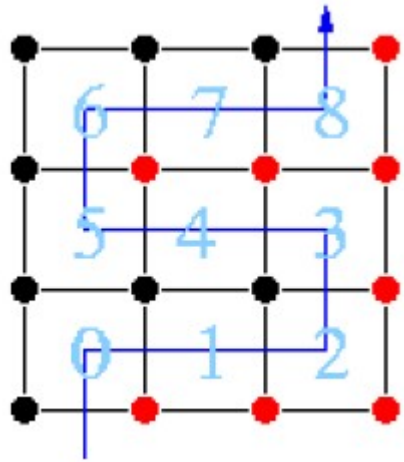

Use of two stacks with a Peano curve on a 2D regular grid

Application of space-filling curves

2. Implementation with respect to cache-efficiency (3)

Consequences:

- Memory behaviour becomes deterministic and processing order is easily inverted.

- The discrete operator has to be decomposed per cell such that the accumulated effect corresponds to the execution of the whole operator after one run over all cells.

Application of space-filling curves

3. Grid partitioning and parallellisation (1)

For running a PDE solver on a parallel computer we need to partition the data and map each block to a processor such that data transfer between the processors is as small as possible.

Multi-dimensional data can be mapped to a one-dimensional sequence using the inverse of a discrete SFC mapping. The points on *I* that are the images of nodes in space can be grouped together and mapped on a processor. We use seperators to form partitions that contain the same number of nodes for perfect load balance.

Application of space-filling curves

3. Grid partitioning and parallellisation (2)

- Set of points: $S = \{x_i \mid x_i \in \Omega\}$

$$S = \bigcup_j \{x_i \mid s_j < f^{-1}(x_i) < s_{j+1}\}$$

$$I = \bigcup_j I_j$$

where I_j of equal workload, gives small seperators $\partial f(I_j) \setminus \partial\Omega$,
in fact quasi-optimal seperator sizes where other partition methods fail.

List of references

[1] Hans Sagan, Space-Filling Curves, Springer-Verlag, 1994.
[2] Michael Bader, Raumfüllende Kurven, Institut für Informatik der Technischen Universität München, 2004.
[3] F. Günther, M. Mehl, M. Pögl, C. Zenger, A cache-aware algorithm for PDEs on hierarchical data structures based on space-filling curves.
[4] Gerhard Zumbusch, Adaptive Parallel Multilevel Methods for Partial Differential Equations.
[5] R. Dafner, D. Cohen-Or, Y. Matias, Context-based Space Filling Curves, 2000.
[6] www.wikipedia.org

Fractal Capacitor

- Quasi fractal geometries can be utilized to increase capacitance per unit area.

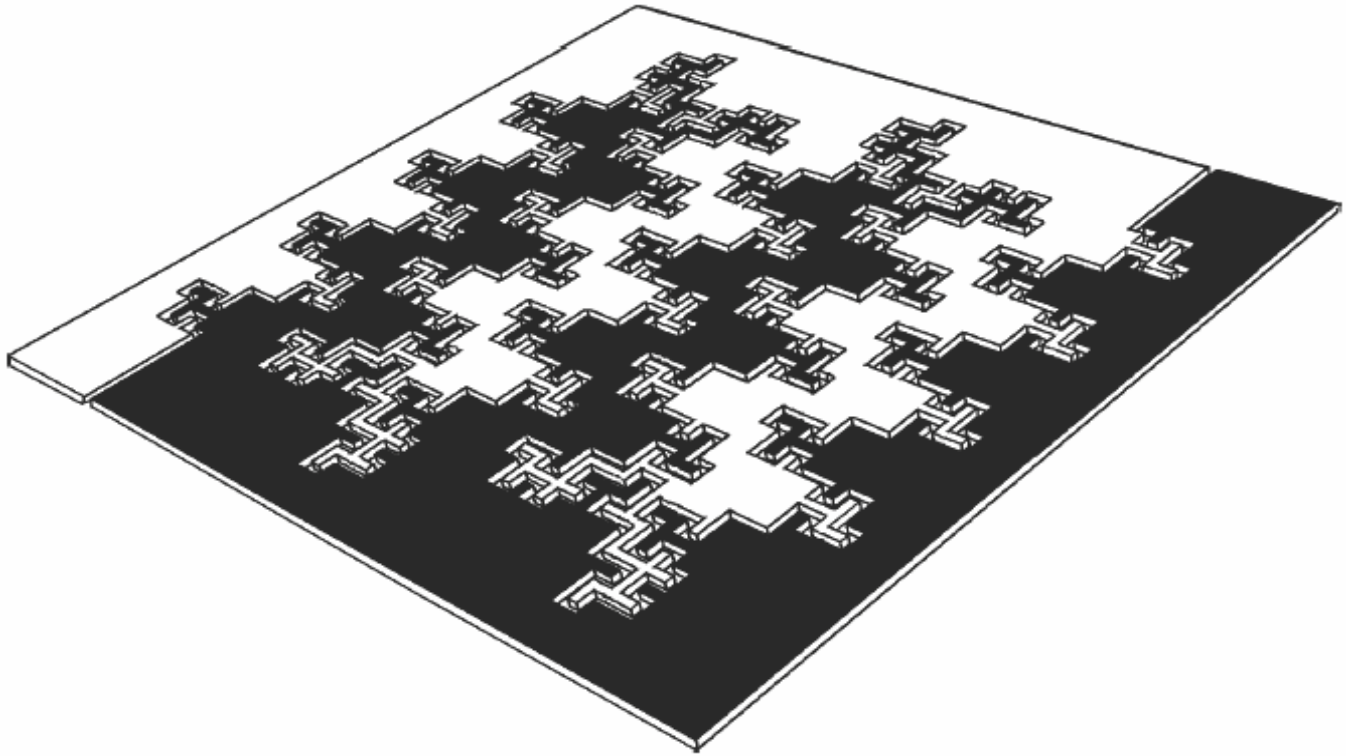

3-D representation of a fractal capacitor using a single metal layer.

Vertical vs. Lateral Flux

- Lateral flux increases the total amount of capacitance.

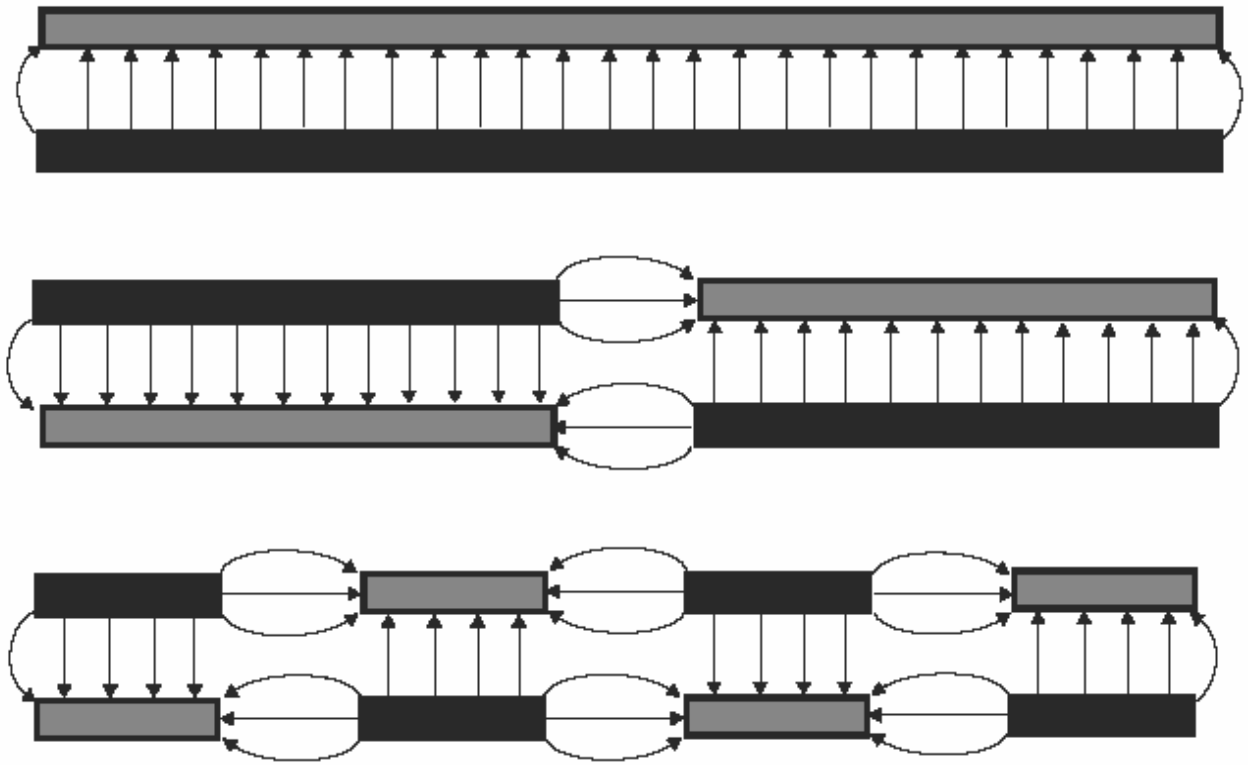

Scaling

- Unlike conventional parallel-plate structures, the capacitance per unit area increases as the process technologies scale.

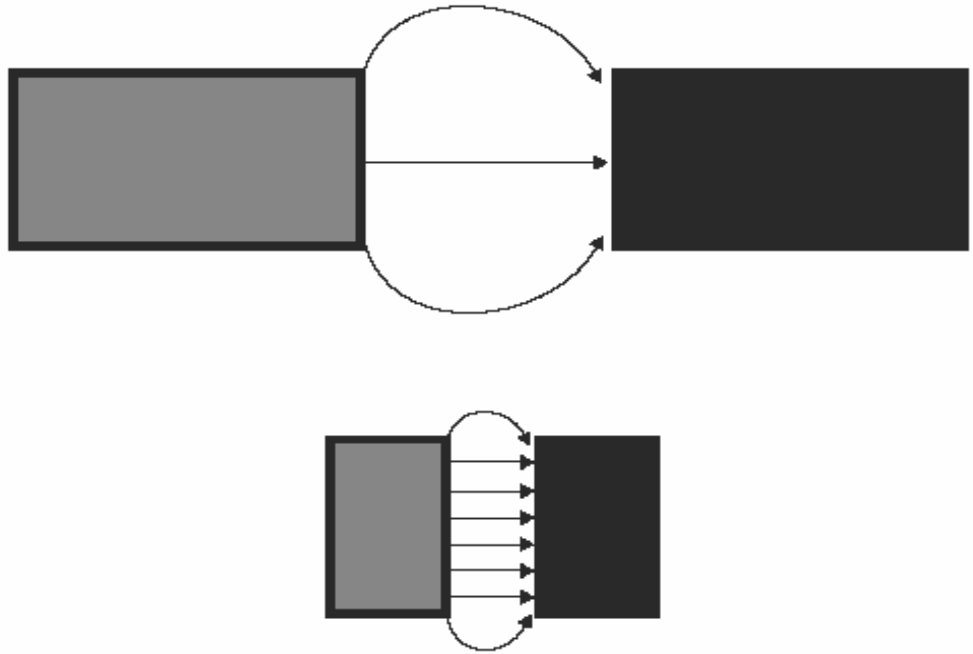

Manhattan capacitor structures

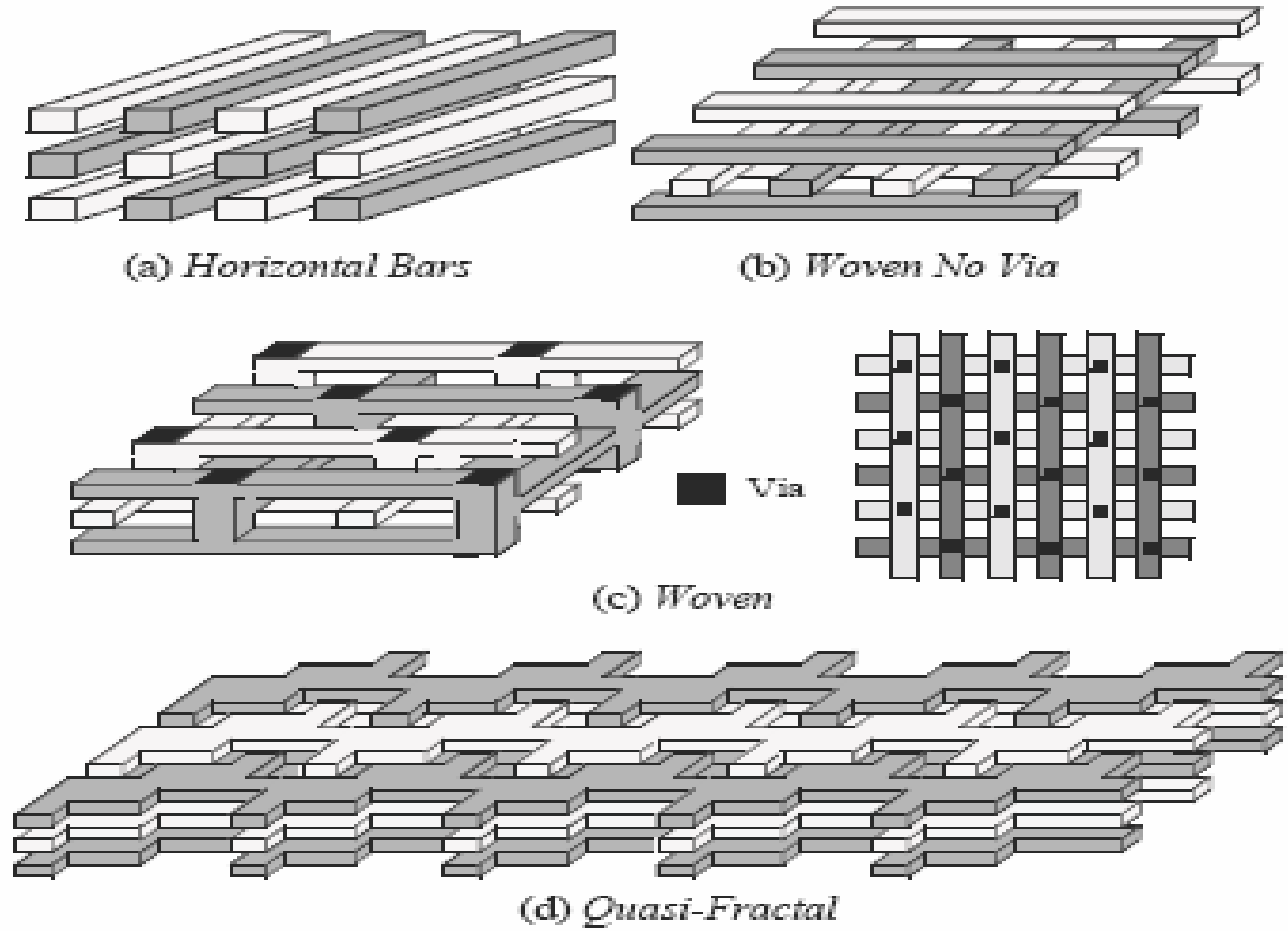

Capacitance Estimation

$$C_{lateral} = K\frac{(\sqrt{A})^{D}}{(w+s)^{D-1}} \times t$$

- *w*: Minimum width of the metal.
- *s*: Minimum spacing between two adjacent strips.
- *A*: Area of the fractal capacitance.
- *t*: Thickness of the metal layers.
- *K*: Proportionality factor that depends on the family of fractals being used.
- *D*: Fractal dimension.

Boost Factor *vs.* Lateral Spacing

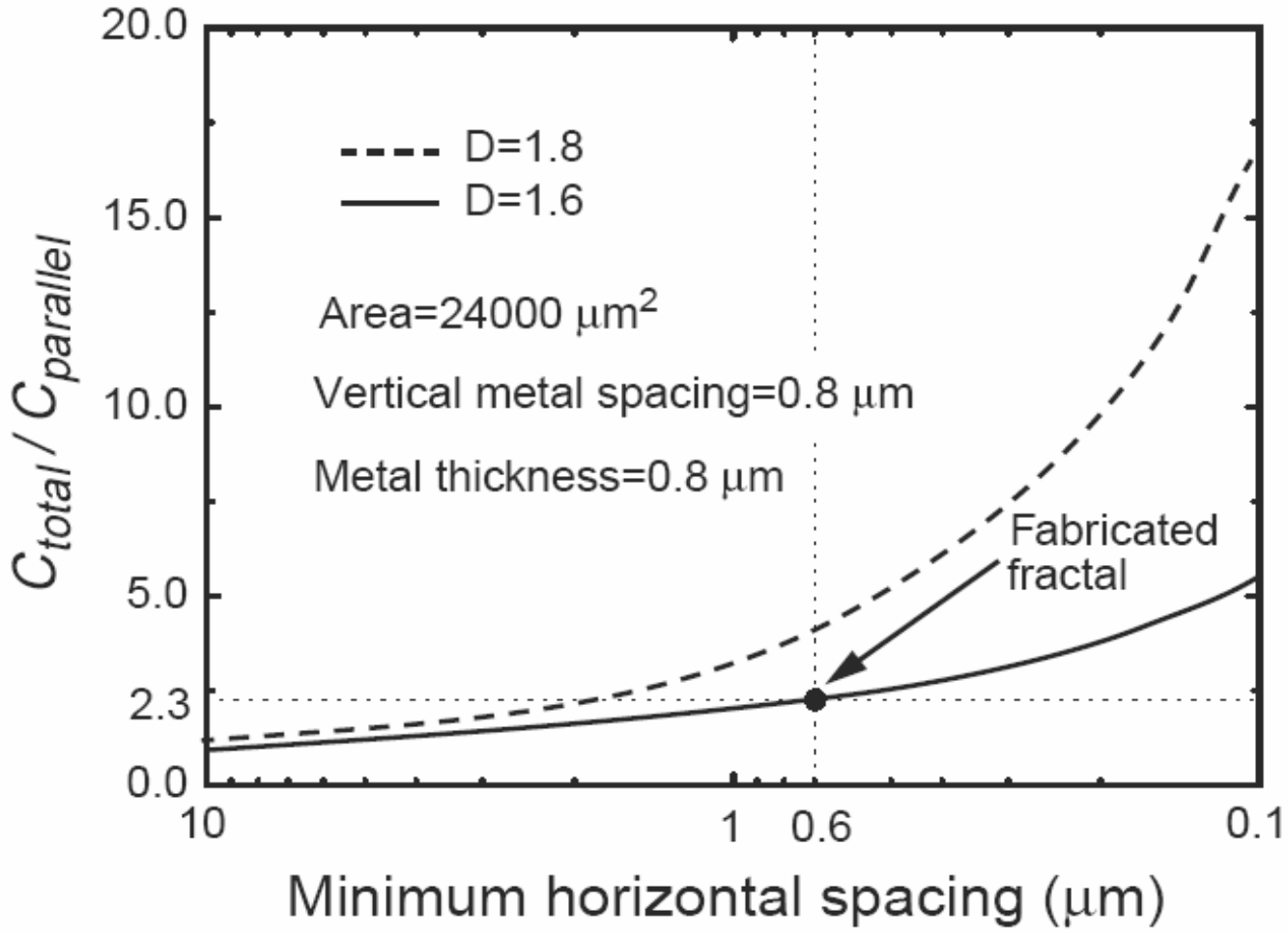

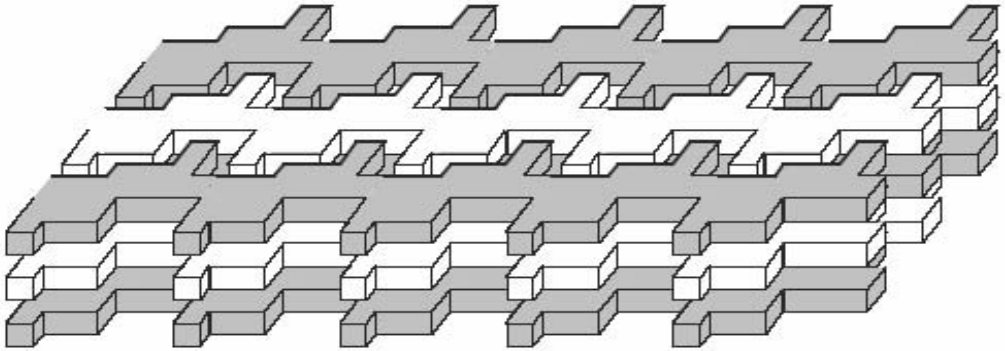

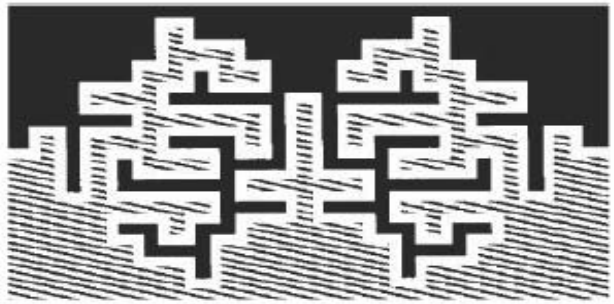

- Quasi-fractal structures maximize periphery to increase field usage,
- Have strong vertical *and* lateral components,
- Time consuming to generate and simulate,
- Look beautiful !

[Samavati, Hajimiri, Shahani, Nasserbakht, and Lee, ISSCC 1998]

Capacitance density comparison

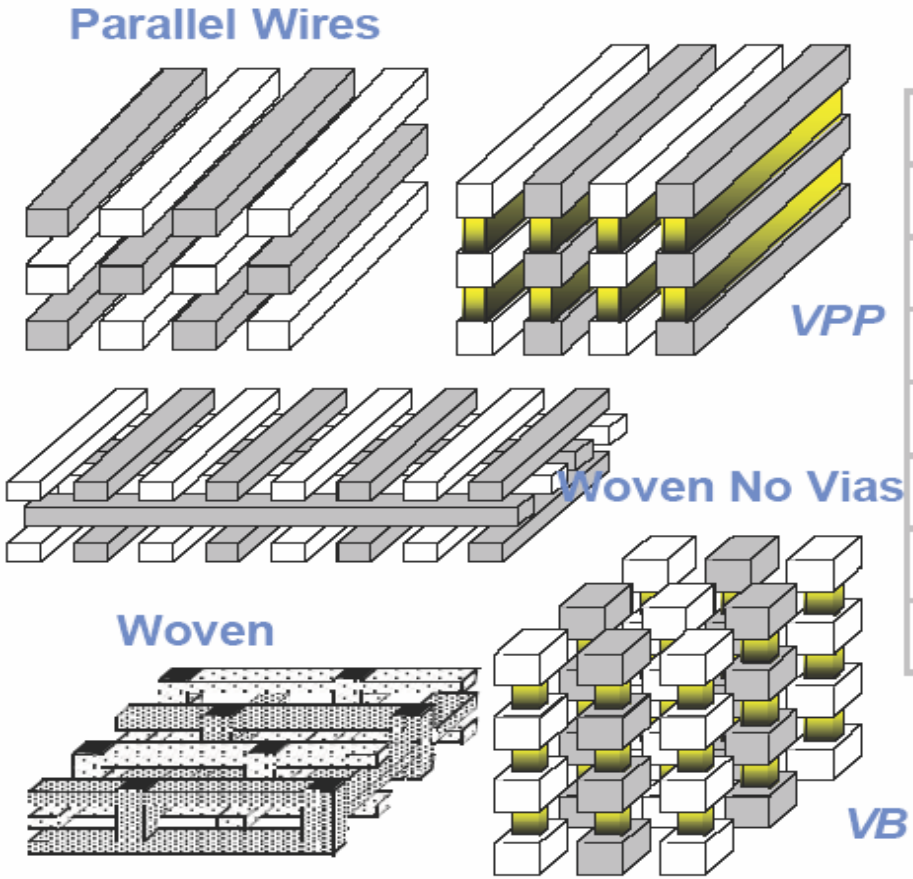

	% TL1	% TL2
Woven	37.0%	52.7%
Woven no Vias	28.3%	40.3%
Parallel Wires	28.3%	40.3%
Quasi-Fractal	17.9%	25.5%
Horizontal PP	0.8%	1.1%
Vertical PP	49.6%	70.7%
Vertical Bars	63.7%	90.8%

[Aparicio and Hajimiri, JSSC March 2002]

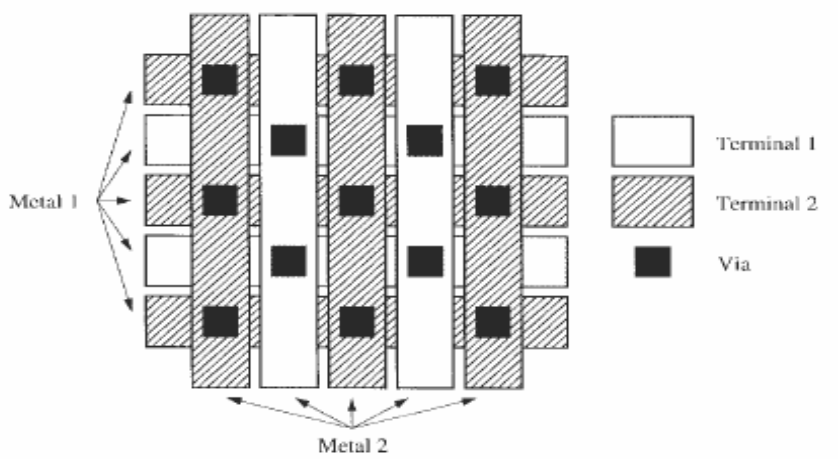
Metal 1
Terminal 1
Terminal 2
Via
Metal 2

Measurement Summary

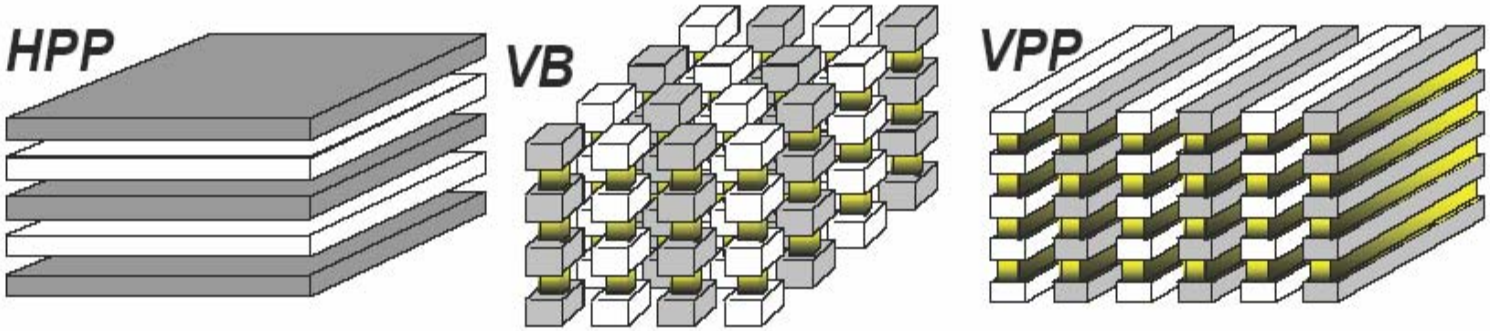

	HPP	VB	VPP	MIM 0.18µ
Average Cap. [pF]	1.095	1.076	1.013	1.057
Cap. Density [aF/µm^2]	203.6	1281.3	1512.2	1100
Cap. Enhancement	1	6.29	7.43	5.40
f_{res} [GHz]	21	37.1	40 <	11
Q (Measured) @1GHz	63.8	48.7	83.2	95

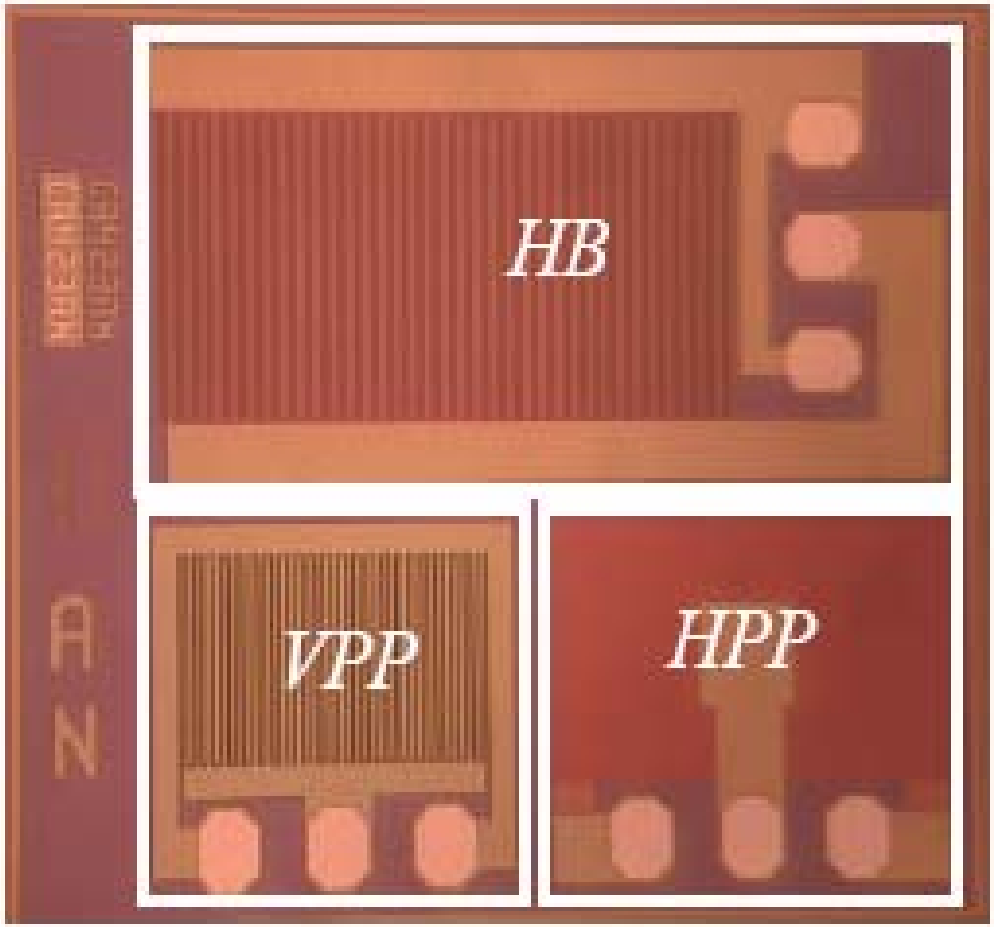
HB
VPP
HPP